Chapter 5

Ozone Response to Aircraft Emissions: Sensitivity Studies with Two-Dimensional Models

Malcolm Ko
Atmospheric and Environmental Research, Inc.
Cambridge, MA

Contributors

D. Weisenstein
Atmospheric and Environmental Research Inc.
Cambridge, MA

C. Jackman, A. Douglass, and K. Brueske
National Aeronautics and Space Administration
Goddard Space Flight Center

D. Wuebbles and D. Kinnison
Lawrence Livermore Laboratory
Livermore, CA

G. Brasseur
National Center for Atmospheric Research
Boulder, CO

J. Pyle and A. Jones
University of Cambridge
United Kingdom

R. Harwood
University of Edinburgh
United Kingdom

I. Isaksen and F. Stordal
University of Oslo
Norway

R. Seals
National Aeronautics and Space Administration
Langley Research Center
Hampton, VA

INTRODUCTION

This chapter presents our first intercomparison/assessment of the effects of a proposed high-speed civil transport (HSCT) fleet on the stratosphere. As an assessment, this report is necessarily interim; it will be followed by a sequence of more detailed assessments and validation studies as part of the High-Speed Research Program (HSRP). These model calculations should be considered more as sensitivity studies, primarily designed to serve the following purposes:

- allow for intercomparison of model predictions;
- focus on the range of fleet operations and engine specifications giving minimal environmental impact; and
- provide the basis for future assessment studies.

The basic scenarios were chosen to be as realistic as possible, using the information available on anticipated developments in technology. They are not to be interpreted as a commitment or goal for environmental acceptability.

The scenarios are minimal, focusing mainly on the emission of NO_x and H_2O, as described under Emissions Scenarios for Supersonic and Subsonic Aircraft. The predicted HSCT fleet could be fully operational by about the year 2015, when the atmospheric concentrations of most trace gases are expected to be different from what they are today. It was decided that the calculations should be performed relative to a background atmosphere for the year 2015. The boundary conditions that define the year 2015 atmosphere are described in the next section. It has been assumed that there will be no reduction in the subsonic fleet with the introduction of the supersonic fleet. Thus, the impact of the supersonic fleet will be compared with the baseline atmosphere, which includes a projected subsonic fleet operating in the year 2015 background atmosphere.

The results from the models are presented in the section, Intercomparison of Model Results. It should be emphasized that the calculations reported in this chapter are performed using gas-phase chemistry only. Heterogeneous chemistry occurring on the global sulfate layer and/or the polar stratospheric clouds (PSCs) could modify the results in a significant way. These effects could be further enhanced if there is an increase in the sulfate layer or an increase in the occurrence of PSCs as a result of the operation of the HSCT. These issues will be discussed under the heading, Concluding Remarks, along with a discussion of how to identify observations that are useful for validating the predicted effects of these reactions in the stratospheric chemistry models.

EMISSION SCENARIOS FOR SUPERSONIC AND SUBSONIC AIRCRAFT

For two-dimensional (2-D) models that simulate the zonal-mean (averaged over longitude) distributions of the trace gases, one must specify the distributions of the emitted materials as functions of latitude, height, and season. The input for the calculations is summarized in Table 1. A brief review of the key parameters is given in this section.

Table 1. Parameters for Aircraft Scenarios

	Subsonic Cruise		Supersonic Cruise
	Short Range	Long Range	
FUEL USE 10^9 (kg/yr)			
	20	150	all cases, 70
CRUISE ALTITUDE thousands ft (km)			
	20-30 (6.1-9.1)	30-40 (9.1-12.2)	Mach 1.6 : 47-57 (14.3-17.4) Mach 2.4 : 55-65 (16.8-19.8) Mach 3.2 : 70-80 (21.3-24.4)
LATITUDINAL DISTRIBUTION OF FUEL USE (%)			
80°N-90°N	0		0.6
70°N-80°N	0.4		0.7
60°N-70°N	2.9		0.7
50°N-60°N	15.7		12.3
40°N-50°N	25.2		28.4
30°N-40°N	31.6		18.4
20°N-30°N	11.0		8.4
10°N-20°N	3.7		6.7
Eq-10°N	2.4		6.3
Eq-10°S	1.7		4.9
10°S-20°S	1.6		4.2
20°S-30°S	1.6		4.0
30°S-40°S	2.0		3.1
40°S-40°S	0.2		1.3
50°S-90°S	0		0
EMISSION INDICES (gm/kg fuel)			
Species (gm mol. wt.)	References		
NO_x as NO_2	(46)	20.7	As specified
H_2O	(18)	1230	1230
CO	(28)	1.1	1.5 (1.2-3.0)
HC as CH_4	(18)	0.2	0.2 (0.02-0.5)
SO_2	(64)	1.1	1.0
CO_2	(44)	3160	3160

Total Fuel Use

The calculations will be performed for supersonic fleets with cruise fuel use of 70×10^9 kg/year. This corresponds to a realistic fleet of approximately 500 or more aircraft, which represents an economically feasible size for the HSCT fleet. Fuel use during takeoff, climb, and descent will be ignored in these calculations.

Latitude Distribution of Cruise Fuel Use

The adopted latitudinal distribution of fuel use is given in Figure 1. A detailed distribution for any specific fleet will, of course, depend on flight routes, anticipated demands between city-pairs, and routing to avoid sonic booms over land. The chosen distribution is based on two independent studies that take into account each of these concerns (1,2). Fuel use is distributed according to projected flight paths, and the emitted materials are assumed to be deposited along the flight paths. No adjustment is made to account for the vertical and meridional transport of the plume that may occur in the first few weeks before the emitted material becomes zonally mixed.

Altitude and Mach Number

Aircraft with particular cruise speeds (Mach numbers) operate most efficiently at specific altitudes. The adopted altitude range for each Mach number is specified in Table 1. The assigned spread in altitude is in accord with possible traffic control and the natural climb of cruise altitudes toward the end of a trip, as the fuel is being used up. Here, we ignore the latitudinal variation of the altitude range of injection.

Fuel use and emissions are assumed to be uniform throughout the year.

Emitted Material

The emission index (EI) for oxides of nitrogen, $EI(NO_x)$, is defined as in chapter 1 as equivalent grams of NO_2 emitted per kilogram of fuel use. The NO_x emitted is typically 90% NO and 10% NO_2, on a molecular basis. This value should be used if a distinction between NO and NO_2 emission is needed. EIs for other species are as specified in Table 1.

Subsonic Fleet

The emissions for the year 2015 subsonic fleet are based on the Boeing B6 references scenario (1). The impact of the subsonic fleet is represented by emissions at two cruise altitudes: 20,000-30,000 ft and 30,000-40,000 ft. The assumed fuel use is 20×10^9kg/year and 150×10^9 kg/year, respectively. Because of an error, some modeling groups were instructed to distribute fuel use for the lower cruise altitude between 0 and 30,000 ft, but this discrepancy makes little difference, since most results are to be examined in term of changes relative to baseline.

The latitudinal distributions of fuel use for the two cruise altitudes are given in Figure 2. For simplicity, we adopt the distribution for the greater fuel use (30,000-40,000 ft) for both cases. Fuel use is assumed to be constant throughout the year. The EIs for the species included in these sensitivity studies are given in the Table 1.

Background Atmosphere

The change in O_3 will be calculated as a percentage change relative to the baseline atmosphere specified in Table 2 (atmosphere in year 2015, with the subsonic aircraft fleet). Note that, if heterogeneous chemistry is active, the model-predicted ozone content of the 2015 atmosphere is particularly sensitive to the chlorine loading in the atmosphere.

Table 2. Boundary Conditions for Atmospheric Composition

Species	Concentration in 1985*	Concentration in 2015+	Comment
CFC-11	220 ppt	260 ppt	The boundary condition for the CFCs is assumed to be half-way between complete phaseout in 2000 (Prather and Watson†, case 1b) and the revised Montreal Protocol.
CFC-12	375 ppt	510 ppt	
CFC-113	30 ppt	70 ppt	
CFC-114	5 ppt	10 ppt	
CFC-115	4 ppt	8 ppt	
CCl4	100 ppt	100 ppt	
HCFC-22	80 ppt	200 ppt	The values for HCFC-22 and CH_3CCl_3 reflect use of other substitutes.
CH_3CCl_3	130 ppt	150 ppt	
Halon-1301	1.7 ppt	6 ppt	
Halon-1211	1.5 ppt	2 ppt	
CH_3Cl	600 ppt	600 ppt	Assumed natural.
CH_3Br	10 ppt	10 ppt	Assumed natural.
N_2O	306 ppb	330 ppb	Assumed increase of 0.25% per year.
CH_4	1600 ppb	2050 ppb	Assumed increase of 15 ppb per year.
CO_2	345 ppm	390 ppm	Assumed increase of 0.45% per year.

*While it is recognized that other boundary conditions affecting tropospheric chemistry such as CO and NO_x, will change with time, it is recommended that each model keeps its present-day reference troposphere unchanged in the simulations.
+The total chlorine content is about 3.7 ppb in the year 2015 atmosphere.
†M.J. Prather, R.T. Watson, Stratospheric ozone depletion and future levels of atmospheric chlorine and bromine, *Nature, 344,* 729-734, 1990.

Scenarios for Supersonic Fleet

Recent modeling results (3-7) showed that the main impact on ozone depends on the total amount of NO_x emitted and the altitude of injection. For fixed fuel use, the calculated ozone response should be related to the EI(NO_x). The Mach number and the EI for NO_x are

used as the only two independent parameters in this set of sensitivity scenarios. The chosen scenarios are shown in the two-parameter space of EI and Mach number in Figure 3.

The recommended model simulations are:

- one baseline simulation (BSE) : background atmosphere + subsonic fleet;
- seven perturbation runs (A through G) : background atmosphere + subsonic fleet + one of the fleets listed in the figure.

Note that cases F, A, and G represent three cases wherein NO_x EI=15 and cruise speeds are Mach 3.2, 2.4, and 1.6, respectively. Cases B, C, and D represent the same set of cruise speeds, with NO_x EI=5. Case E (EI=45) represents a fleet with present-day technology flying at Mach 2.4.

INTERCOMPARISON OF MODEL RESULTS

The modeling groups that participated in the intercomparison are:

- AER — Atmospheric and Environmental Research Inc.: M. Ko and D. Weisenstein
- GSFC — NASA Goddard Space Flight Center: C. Jackman, A. Douglass, and K. Brueske
- LLNL — Lawrence Livermore Laboratory: D. Wuebbles and D. Kinnison
- NCAR — National Center for Atmospheric Research: G. Brasseur
- CAMED-P — University of Cambridge and University of Edinburgh: J. Pyle, R. Harwood, and A. Jones
- OSLO — University of Oslo: I. Isaksen, F. Stordal

The procedure for this intercomparison assessment made use of the infrastructure set up for previous model intercomparison workshops (8). Dr. Robert Seals, Jr., of the Upper Atmosphere Data Program (UADP) at NASA Langley Research Center is in charge of the database for the model results. Model results in digital format were sent to the database in standard UADP format. Each modeling group was asked to send at least 4 months (March 15, June 15, September 15, and December 15) of latitude-height fields of NO_y, H_2O, Cl_y, O_3, and noontime $NO + NO_2$ (NO_x), along with latitude-season (12 months) of the column abundance of O_3 for each simulation.

It was agreed that the modelers would use only gas-phase chemistry for the first set of runs. However, as part of the later UNEP/WMO Ozone Assessment, they were encouraged to add heterogeneous chemistry for later studies and the 1992 HSRP/AESA annual meeting will examine these studies with the new heterogeneous, sulfate-layer chemistry. Only the emissions for NO_x and H_2O are to be used in the simulations. The emissions for CO, hydrocarbons (HC), SO_2, and CO_2 are included in Table 1 for reference, so that sensitivity studies could be made with some models. Preliminary estimates have confirmed that their impacts are minor.

Background Atmosphere

The calculated column abundances of ozone (O_3) for the 2015 atmosphere that include the subsonic fleet from the models are shown in Figure 4. The calculated column abundances of O_3 are quite similar, within 20% of each other. Previous model intercomparison (8) showed that the simulated O_3 abundances for the 1985 atmosphere are within 20%. Model results not shown here indicated that the ozone column for the 2015 atmosphere is within 2% to 5% of the 1985 atmosphere. The consistency among the model results is encouraging. At the same time, one must remember that one is interested in calculated O_3 changes of about a few percent.

The "good" agreement among the models should not be taken at face value as validation of the model results. It has been noted (9) that the ozone decrease over the past decade predicted by models using gas-phase chemistry is smaller than the observed trend. A possible explanation is the omission of the effect associated with enhanced concentrations of the active chlorine species produced by heterogeneous reactions occurring on PSCs and the global aerosol layer.

The concentration of O_3 in the high-latitude lower stratosphere is controlled by a balance between transport and local photochemical removal. The fact that the simulated O_3 concentrations in different models all bear some semblance to the observations does not necessarily imply that the simulated transport rates and chemical removal rates in different models are approximately the same. Similar O_3 distributions may be obtained by combinations of different transport and photochemical removal terms. As a result, the response of the O_3 to changes in the chemical forcing calculated in different models may be very different.

Comparison of the mixing ratios of several species in the high latitude lower stratosphere is shown in the Table 3. Recognizing that the photochemical lifetime of O_3 in the lower stratosphere is on the order of months, we decided to pick a sufficiently large region poleward of 40°N and from z^*= 12 km to z^*= 28 km. The altitude variable z^* is expressed in kilometers and is defined in terms of pressure as $z^* = 16 \log_{10} (1000/p)$, where p is in mb. The values in Table 3 are reported as average mixing ratios, which are defined as the total number of molecule of the species in the region, divided by the total number of air molecules in the same region. In other words, it is the average mixing ratio weighted by the local air-density. In addition, the values reported are averages of the monthly values used to represent annual averages.

Table 3. Average Mixing Ratios for the 2015 Atmosphere*

Model	H_2O (ppmv)	Cl_Y (ppbv)	NO_y (ppbv)	$NO+NO_2$ (ppbv)	NO_x/NO_y	O_3 (ppmv)
AER	5.8	1.2	6.5	1.2	0.18	1.8
CAMED-P	9.5	1.1	5.9	1.7	0.16	1.8
GSFC	5.8	0.72	3.6	0.76	0.21	1.7
LLNL	14.6	0.94	5.2	1.2	0.23	1.8
NCAR	3.7	0.97	7.7	2.2	0.29	1.6
OSLO	N/A	0.91	5.1	1.1	0.22	N/A

*Values given in the table are annual averages over the region between 40°N and 90°N; z^*=12 km to 28 km.

Note that the H_2O, Cl_y and NO_y concentrations in the lower stratosphere are quite different among models. The degree to which the results from the different models agree with each other may depend on the size of the region chosen for the analysis. For instance, the large value of H_2O in the LLNL model is probably due to the fact that the chosen region includes part of the troposphere in that model. In spite of the great differences in the calculated NO + NO_2 among the models, the calculated O_3 is quite similar. This suggests that there may be significant differences in the functional dependence of O_3 on the calculated photochemical removal rates in the different models.

For further comparison of model results, see reference 8.

Scaling Estimate for Trace Gas Perturbation

With assumed fuel use at 70×10^9 kg/year, a "ball park" estimate of the expected local change in concentration for an inert tracer resulting from the aircraft emissions is about 0.5 ppbv for an EI of 1. In the case of NO_y, where EI is on the order of 10, the expected change in concentration is up to a few ppbv, while for H_2O, an EI of 1000 would cause an increase of about 0.5 ppmv.

Based on the EI values given in Table 1, the biggest changes, when expressed as percentages of the background concentration, are for NO_y and H_2O. We will examine the changes in H_2O and NO_y for each case and compare the residence times for each species in the different models.

Change in NO_y

Table 4 shows the calculated changes in content of NO_y above z^*= 6 km in units of kiloton (N). An annual fuel use of 70×10^9 kg/yr would result in an injection rate for NO_y of 107 kiloton (N)/yr for EI of 5; 320 kiloton (N)/yr for an EI of 15; and 959 kiloton (N)/yr for an EI of 45. One can take the change in stratospheric content of NO_y in Table 4 and divide by the corresponding injection rates to obtain stratospheric residence times for the injected NO_y in each of the cases. The results from each model showed that this residence time is independent of EI.

Table 4. Model Calculated Change in Global Content of NO_y above 6 km at Steady State [kiloton (N)]

	EI = 5			EI = 15			EI = 45
Mach No./Case	3.2/B	2.4/C	1.6/D	3.2/F	2.4/A	1.6/G	2.4/E
AER	233	172	63	875	491	184	1472
CAMED-P				834	503	245	
GSFC	184	135	80	528	393	245	1166
LLNL	184	135	59	564	393	172	1166
NCAR	172	113	77	528	344	233	1018
OSLO	233	120	53	675	356	160	1067

The values are given in Table 5 as functions of injection heights or Mach numbers. Note that a large number for residence time implies that the emitted NO_y is retained in the stratosphere for a

longer period of time, so that more NO_y will be added to the stratosphere at steady state for a particular emission rate. As a result, more O_3 will be removed for the same emission.

The results in Table 5 indicate that all models showed different residence times for different injection heights. There is no consistent ranking of the models that applies to all injection heights. The large difference for the Mach 1.6 case is probably due to the difficulty in obtaining an accurate number for the change in NO_y, which is about 10% of the background.

Table 5. Stratospheric Residence Time (Years) of Injected NO_y

Model	Mach 3.2	Mach 2.4	Mach 1.6
AER	2.1	1.5	0.6
CAMED-P	2.6	1.5	0.8
GSFC	1.7	1.2	0.8
LLNL	1.8	1.2	0.5
NCAR	1.7	1.1	0.7
OSLO	2.1	1.1	0.5

The model-calculated changes in NO_y are shown in Figures 5(a)-(g). For case F (Mach 3.2 and EI=15), most models showed an increase of 1 ppbv extending into the way to the southern hemisphere. The CAMED-P model indicated an increase of 2 ppbv. For case A (Mach 2.4 and EI=15), the increase in the southern hemisphere is about 0.5 ppbv, with the maximum local increase in the northern latitude ranging from 2-4 ppbv. In case G (Mach 1.6, EI=15), most models show an increase in the southern hemisphere of about 0.1 to 0.2 ppbv, with the maximum in the northern latitude ranging from 1-1.4 ppbv. The GSFC model is particularly efficient in exporting the material to the southern hemisphere for the Mach 1.6 injection, resulting in an increase of 0.4 ppbv.

The increases in burden of NO_y in the northern lower stratosphere (i.e., 40°N-90°N, 12-28 km, annual average) are given in Table 6. This region is chosen because, based on the photochemical and transport lifetimes of ozone in the lower stratosphere, the changes in ozone in the northern mid-latitudes are expected to be influenced by the changes in photochemical balance in this whole region. If the model can distribute the injected NO_x out of this region, the ozone decrease in the northern hemisphere will be smaller. Table 7 gives the ratio of the increase in regional NO_y abundance (Table 6) to the increase in global burden (Table 4). A smaller value in Table 7 implies that the model is more efficient in exporting the emitted material out of the local region. Values given in Table 7 indicated that the AER model is consistently among those that is least efficient in exporting the NO_y, while the CAMED-P model is the most efficient. Other models show different efficiencies, depending on cruise altitude.

Change in H_2O

Calculated changes in H_2O for case F (Mach 3.2) are shown in Figure 6. Note that, for H_2O, cases B, C, and D are identical to cases F, A, and G, respectively, since there is no change in EI(H_2O) between the two sets. The changes in H_2O are expected to be similar to those for NO_y in the lower stratosphere, where the photochemical removal time for both species is relatively long. They differ in the upper stratosphere, in that the photochemical removal of NO_y is more efficient. The changes in mixing ratio are: 0.2-0.4 ppmv in the NCAR model; 0.4-0.6 ppmv in the AER and LLNL models; and 0.6-0.8 ppmv in the CAMED-P model.

Table 6. Model Calculated Increases in the Burden of NOy [kiloton (N)] in the Region 40°N-90°N, 12-28 km, Annual Average

	EI = 5			EI = 15			EI = 45
Mach No./Model	3.2/B	2.4/C	1.6/C	3.2/F	2.4/A	1.6/G	2.4/E
AER	94	67	25	281	196	74	580
CAMED-P				290	159	70	
GSFC	70	44	23	215	131	69	402
LLNL	68	42	22	206	122	62	374
NCAR	69	41	27	206	122	81	374
OSLO	80	45	22	243	131	51	402

*Expressed as an average mixing ratio in parts per billion by volume for the region.

Table 7. Rates of Changes in NOy Regional Abundance Versus Global Abundance

Model	Mach 3.2	Mach 2.4	Mach 1.6
AER	0.41	0.40	0.40
CAMED	0.35	0.32	0.29
GSFC	0.40	0.34	0.29
LLNL	0.37	0.32	0.36
NCAR	0.39	0.37	0.35
OSLO	0.35	0.37	0.42

It is harder to get quantitative results from the H_2O database because it is difficult to define a meaningful region that excludes the troposphere in all the models. Moreover, modeling H_2O in current stratospheric models involves some uncertain assumptions about the microphysical control of H_2O at the tropopause.

Ozone Column Response

Except for the CAMED-P model, the transport circulation and temperatures in the models are fixed so that the effects of dynamic feedbacks are ignored. Thus, changes in O_3 represent responses to modifications in the chemical removal rates resulting from aircraft emissions. Previous modeling results (3-5) showed that the impact from H_2O emission alone is small. Thus, in this discussion, we will concentrate on the sensitivity of the O_3 response to changes in active nitrogen species ($NO+NO_2$).

The calculated changes in column ozone are shown in Figures 7(a)-(g). The calculated changes in global ozone content are summarized in Table 8. The following observations can be made from the results.

- There is no consistent ordering of the calculated global O_3 decrease among the models. The ordering is different, depending on Mach numbers.

- In the northern hemisphere, the AER, OSLO, and CAMED-P model gave the largest calculated ozone decreases for all cases. The results from the rest of the models were quite similar to the results from GSFC and slightly larger than those from LLNL and NCAR. The spread between the two groups was about a factor of 2.

- In the tropics, the results were similar in all models, except for CAMED-P, which showed a large decrease in the tropics. For case F, all models but CAMED-P showed a decrease of -2%; the CAMED-P model showed -4%. For case A (Mach 2.4 and EI=15), the OSLO model showed a calculated increase in the tropics, while other models calculated a decrease of about -1%. For case G, the AER model and the LLNL model calculated a small increase in the tropics, while the GSFC, NCAR, and CAMED-P model calculated a decrease of -0.4%. The predicted decreases in case E from AER and OSLO were smaller than from the other models.

- In the southern hemisphere, the GSFC and CAMED-P model consistently predicted the largest decrease in ozone. The difference among the models is largest for the Mach 1.6 case.

Table 8. Calculated Decrease in Global Total O_3 (%)

	EI = 5			EI = 15			EI = 45
Mach No./Case	3.2/B	2.4/C	1.6/D	3.2/F	2.4/A	1.6/G	2.4/E
AER	1.2	0.61	0.11	4.3	2.1	0.40	7.5
CAMED-P				5.3	2.5	0.72	
GSFC	1.2	0.50	0.20	4.1	1.7	0.67	5.9
LLNL	0.9	0.50	0.085	3.4	1.7	0.29	6.1
NCAR	0.78	0.31	0.14	3.5	1.4	0.62	4.7
OSLO	1.2	0.15	0.01	4.1	0.72	.002	3.5

Changes in Local O_3 Concentrations

The percent changes in local O_3 for March are shown in Figures 8(a)-(g).

- All models showed large decreases in the region north of 30°N, between 10 and 25 km, where most of the NO_x emissions are deposited.

- Calculations of behavior in the troposphere may depend on the choice of the boundary condition for O_3 in the models. With a fixed mixing boundary condition, the AER model showed slight increases in the troposphere for the southern hemisphere in all cases. In the NCAR model, the increase in tropospheric O_3 is limited to a small area in the tropics. The LLNL and GSFC models predicted an increase only for the Mach 1.6 case.

- The AER, GSFC, LLNL, and CAMED-P models showed increases in the tropical lower stratosphere between 20 and 30 km. The region of increase is most extended for the GSFC model.

- The extent to which the southern lower stratosphere is affected in each model is related to how efficiently NO_y is transported to the southern hemisphere. The CAMED-P model, which has the most efficient global distribution of the emitted NO_y, showed the largest decrease in the south, while the AER model showed the smallest.

Analysis of Ozone Loss

The photochemical removal rate for O_3 caused by the catalytic NO_x cycle is proportional to the concentration of $NO_x = (NO + NO_2)$ calculated in the models. Thus, the increase in the photochemical removal rate is proportional to the increase in NO_x. Table 9 gives the calculated changes in NO_x from the models in the northern lower stratosphere (40°N-90°N, 12-28 km, annual average). Since the NO_x/NO_y ratios are different in different models, it is not surprising

Table 9. Changes in NO_x (= NO + NO_2, ppbv) (40°N-90°N, 12-28 km, Annual Average)

	EI = 5			EI = 15			EI = 45
Mach No./Case	3.2/B	2.4/C	1.6/D	3.2/F	2.4/A	1.6/G	2.4/E
AER	0.16	0.12	0.067	0.67	0.41	0.23	2.1
CAMED-P				1.2	0.68	0.34	
GSFC	0.20	0.13	0.073	0.66	0.42	0.23	1.4
LLNL	0.18	0.13	0.064	0.68	0.41	0.20	1.5
NCAR	0.19	0.14	0.11	0.80	0.54	0.39	1.9
OSLO	0.27	0.14	0.076	0.91	0.48	0.25	0.91

*Expressed as average mixing ratio parts per billion by volume in the region.

that the changes in NO_x do not scale as changes in NO_y. There is actually a repartition of the nitrogen species, in that the ratio changes if the HSCT is operating. The shift in partition is reflected by the increase in the NO_x/NO_y ratio of about 20% for EI = 15 flights and 5% for EI = 5 flights.

The response of O_3 to increases in NO_x depends on how dominant the NO_x cycle is in determining local O_3 concentration and whether changes in NO_x can significantly perturb the other chemical cycles. Preliminary analysis, based on results from gas-phase chemistry, indicates the impact of the other chemical cycles is small and that O_3 is responding to the change in the NO_x cycle. The percent changes of O_3 averaged over northern latitudes are tabulated in Table 10. The corresponding percent change in NO_x is given in Table 11. One can define an O_3 sensitivity index as the percent change in O_3 divided by percent change in NO_x. Again, we found this result to be nearly independent of EI. The values, which are tabulated as functions of Mach numbers, are given in Table 12; they can be interpreted as ratios of the chemical removal

rate from the NO_x cycle to the total removal rate (i.e., the sum of chemical removal rates from all cycles and the removal rate by transport). Note that if O_3 is completely controlled by NO_x chemistry, the index would be 1. However, it should be noted that the converse is certainly not true. A value of 1 would not necessarily imply that ozone is completely controlled by NO_x.

Table 10. Changes in Ozone (%) (40°N-90°N, 12-28 km, Annual Average)

	EI = 5			EI = 15			EI = 45
Mach No./Case	3.2/B	2.4/C	1.6/D	3.2/F	2.4/A	1.6/G	2.4/E
AER	-3.4%	-1.7%	-0.43%	-13%	-6.3%	-1.5%	-21%
CAMED-P				-13%	-6.0%	-2.0%	
GSFC	-3.2%	-1.1%	-0.4%	-11%	-3.8%	-1.4%	-13%
LLNL	-2.0%	-1.1%	-0.25%	-7.9%	-3.7%	-0.85%	-13%
NCAR	-2.1%	-0.82%	-0.38%	-9.6%	-3.6%	-1.6%	-12%
OSLO	NA	NA	NA	NA	NA	NA	NA

Table 11. Changes in NO_x (%) (40°N-90°N, 12-28 km, Annual Average)

	EI = 5			EI = 15			EI = 45
Mach No./Case	3.2/B	2.4/C	1.6/D	3.2/F	2.4/A	1.6/G	2.4/E
AER	14%	10%	6%	57%	42%	19%	82%
CAMED-P				72%	40%	20%	
GSFC	26%	17%	9%	86%	54%	30%	188%
LLNL	5%	10%	5%	56%	34%	16%	124%
NCAR	9%	6%	5%	35%	24%	18%	86%
OSLO	25%	13%	6%	82%	43%	22%	156%

Table 12. Sensitivity Index for Changes in Ozone Relative to NO_x

Model	Mach 3.2	Mach 2.4	Mach 1.6
AER	-0.22	-0.15	-0.08
CAMED	-0.18	-0.15	-0.1
GSFC	-0.13	-0.07	-0.05
LLNL	-0.14	-0.11	-0.05
NCAR	-0.27	-0.15	-0.09
OSLO	NA	NA	NA

Nonetheless, the values defined in Table 12 provide an indication of the sensitivity in each model. The values in the table are on the order of -0.13 to -0.27 for Mach 3.2 injection; -0.07 to -0.15 for Mach 2.4 injection; and -0.05 to -0.1 for Mach 1.6 injection. For Mach 3.2 and Mach 2.4, the AER and NCAR models have the greatest sensitivity. The sensitivity in the GSFC model is particularly small for Mach 2.4.

The differences in the O_3 response can be attributed to the following factors. The CAMED-P results showed the largest increase of both NO_x and NO_y, because the long residence time allows the emitted material to build up over time. The AER results show large O_3 depletion at Mach 2.4 and 3.2 because of the great sensitivity of O_3 to increases in NO_x. The sensitivity index in the NCAR model is just as great (or greater) compared with the AER model, but the O_3 response is tempered by a smaller residence time for the emitted NO_x. Thus, differences in O_3 sensitivity are seen to arise out of differences in the amount of NO_x retained in the stratosphere, as well as the differing degrees to which O_3 is controlled by NO_x chemistry in the lower stratosphere. These differences must be examined and resolved in a way that allows us to select one class of models over another. HSRP is currently sponsoring a major international comparison among models that extends the model-model comparison of 1988 to a suite of model-measurement tests.

CONCLUDING REMARKS

Similarities and Differences Among the Models

It is encouraging that the results within each individual model all show similar dependence on EI for NO_x and cruise altitudes. Thus, all the calculated impacts on O_3 are greater for larger EI and higher cruise altitudes. At the same time, the magnitudes of the calculated O_3 changes differ by as much as a factor of 2. The analysis presented in Analysis of Ozone Loss suggests that the differences can be understood in term of the residence time (Table 5) and O_3 response sensitivity factor (Table 12) peculiar to each model. One must look for observations that can help define these quantities in the current atmosphere.

Validation of Models

There is a sizable database for validating model results. However, the validation of model-predicted response of O_3 to perturbations must go beyond mere comparison of observed and calculated species concentrations. One should try to identify diagnostic quantities from models and observations that are useful for testing the mechanisms that control the O_3 concentrations.

The discussion in the section, Analysis of Ozone Loss, identified the residence time (i.e., tracer dispersion) and the O_3 response sensitivity index to NO_x as two key parameters that characterize the calculated O_3 response. The ^{14}C data from atmospheric nuclear tests seem ideally suited for deriving residence times for comparison with model results. Other data, such as those on ^{238}Pu derived from satellite reentry, may also be useful. Analysis of data for H_2O, O_3, and NO_y near the tropopause may provide clues to the actual mechanisms responsible for the troposphere/ stratosphere exchange rate. To get a handle on the O_3 sensitivity, one can use measurement programs designed to provide simultaneous observations of many species [e.g., such as Atmospheric Trace Molecule Spectroscopy (ATMOS), balloon measurement campaigns, and aircraft campaigns] to provide directly measured or derived concentrations for the radical species, to define the local chemical removal rates for ozone. Getting a handle on the removal rate by transport is much more difficult. Application of the data assimilation technique

to derive transport wind fields from observations may serve as a starting point for deriving transport fluxes of O_3 on the lower stratosphere.

Other Issues

Recent reviews (6,7) highlighted the various components that should be included in future HSRP modeling efforts. We would like to emphasize two important uncertainties that have not been addressed in the calculations reported in this chapter.

Plume dispersion and plume chemistry

The source function for the emitted materials used in the calculations is assumed to have the same latitude-height distribution as the flight paths, and the chemical composition is assumed to be identical to that of the emission at the tailpipe. Plume subsidence and subsequent dispersion in the first few weeks before the emitted materials become zonally mixed could provide an effective distribution of sources that differs from the flight paths. Chemical transformation, occurring homogeneously and heterogeneously, may alter the composition of the materials.

Heterogeneous chemistry in the atmosphere

The O_3 responses shown here were calculated assuming gas-phase reactions only. Heterogeneous reactions occurring on PSCs or on the global sulfate layer could change these responses in a significant way. In this context, one must also consider the possibility that operation of the HSCT may increase the occurrence of PSCs and the loading and size distribution in the sulfate layer. Future assessments, going beyond this initial intercomparison/assessment, will have to include predictions with models that (1) determine parameters for the effects of heterogeneous chemistry and (2) have been rigorously compared with observations of today's stratosphere.

ACKNOWLEDGMENTS

Many people contributed to the success of this effort. These include various committees that helped to set up the ground work and emission scenarios, all modeling groups that delivered the model results in a timely fashion, the Upper Atmosphere Data Program at NASA Langley, and all those who helped to prepare and review this chapter. Special thanks go to Debra Weisenstein at AER, who helped to develop some of the software for compiling the results; and to Linda Hunt and Karen Sage from NASA Langley, who generated the numbers for the tables and the graphics in this chapter.

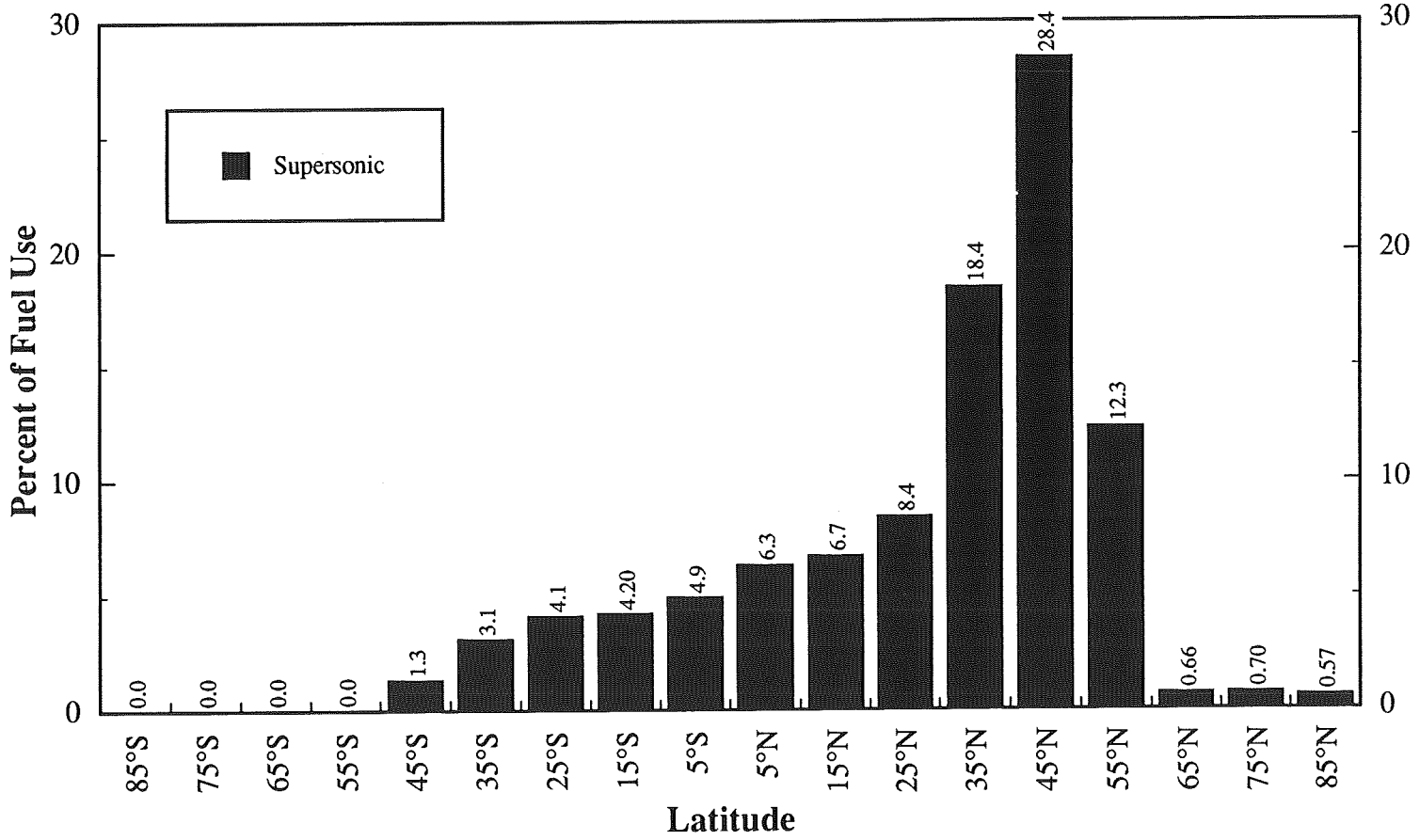

Figure 1. Latitudinal distribution of cruise fuel use for the supersonic fleet, showing the percentage of total fuel use at each latitude.

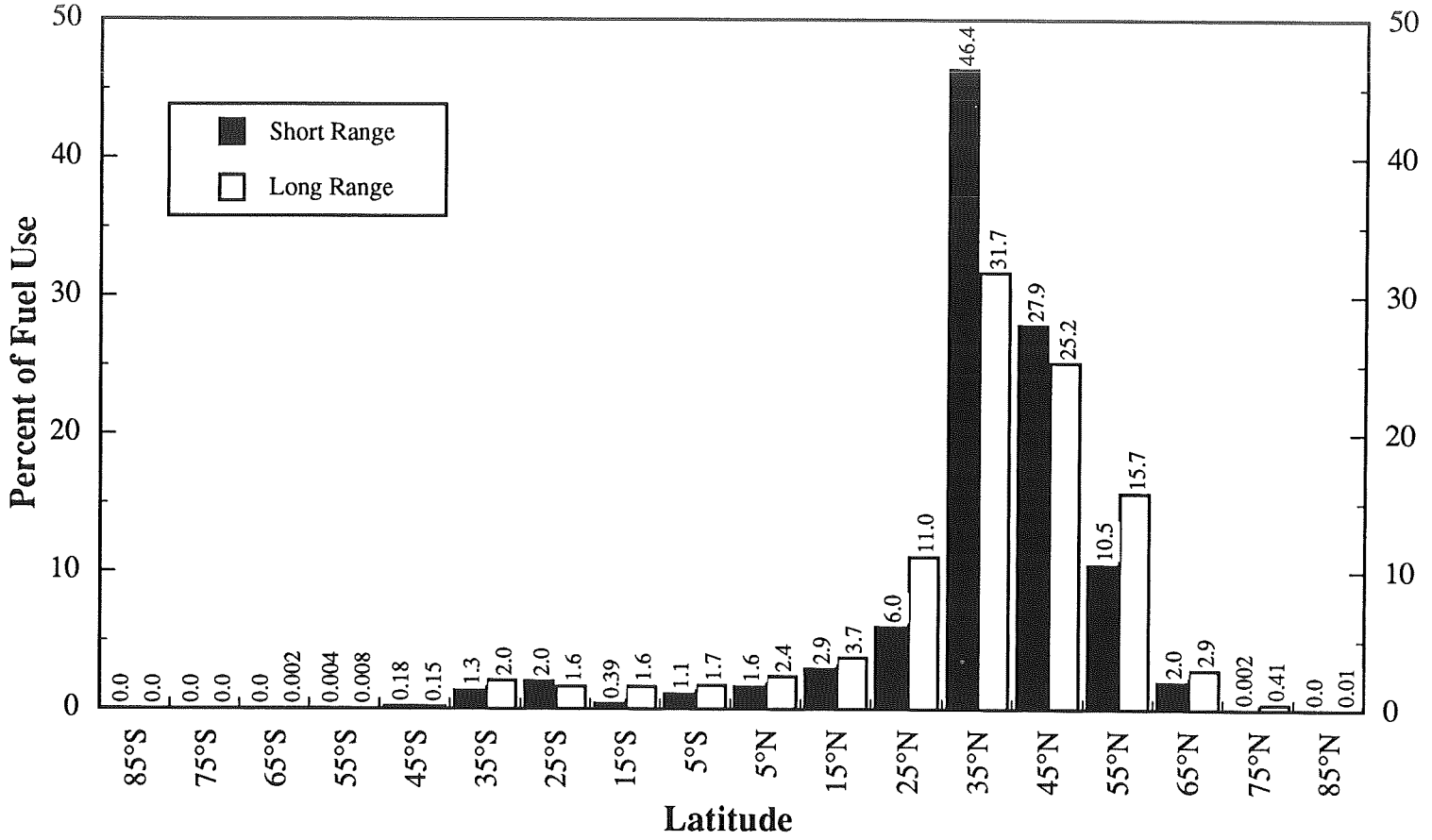

Figure 2. Latitudinal distribution of fuel use for the subsonic fleet at two cruise altitudes, showing the percentage of total fuel use at each latitude.

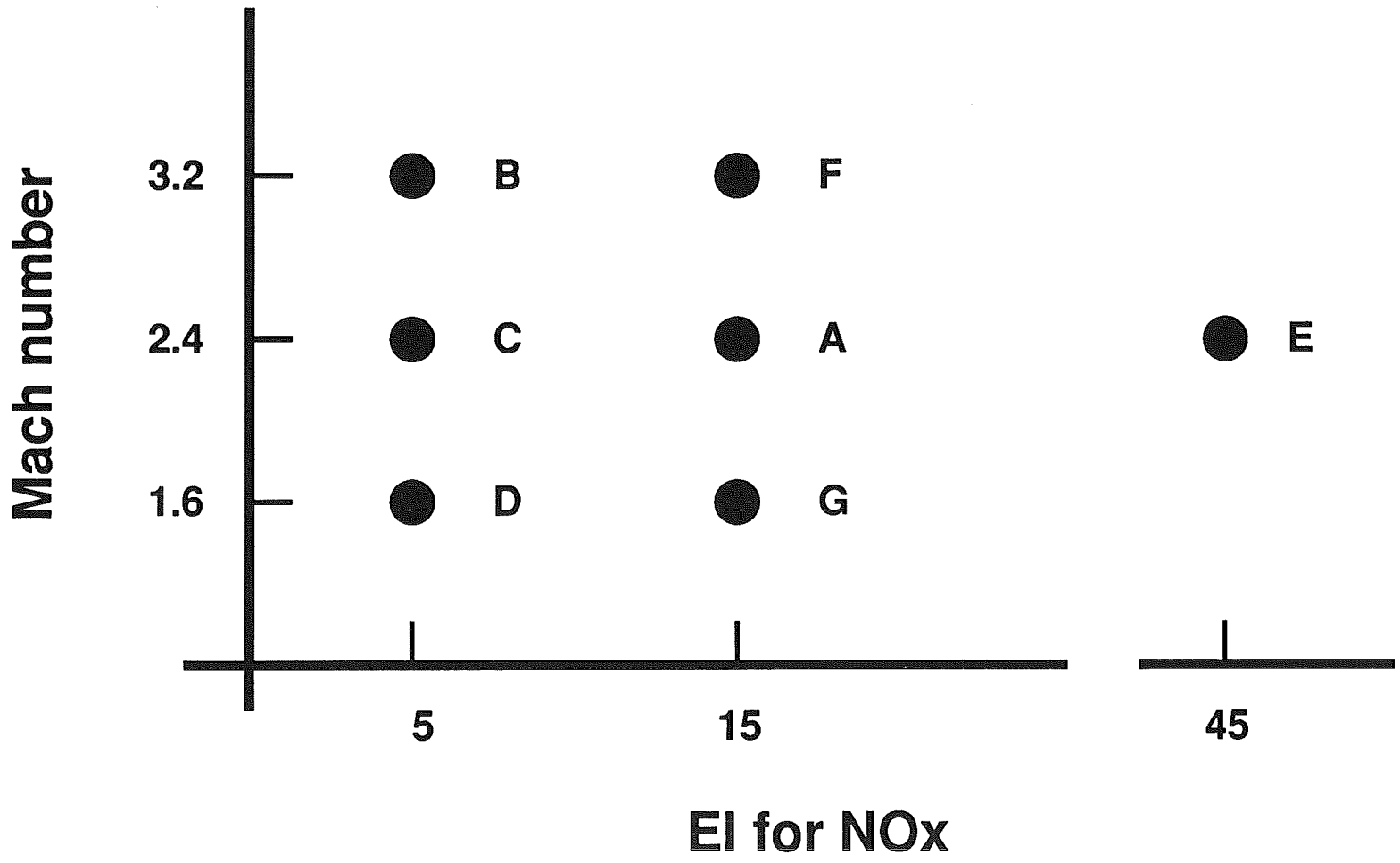

Figure 3. Schematic diagram showing the scenarios in the two-parameter space of EI for NO_x and cruise altitudes.

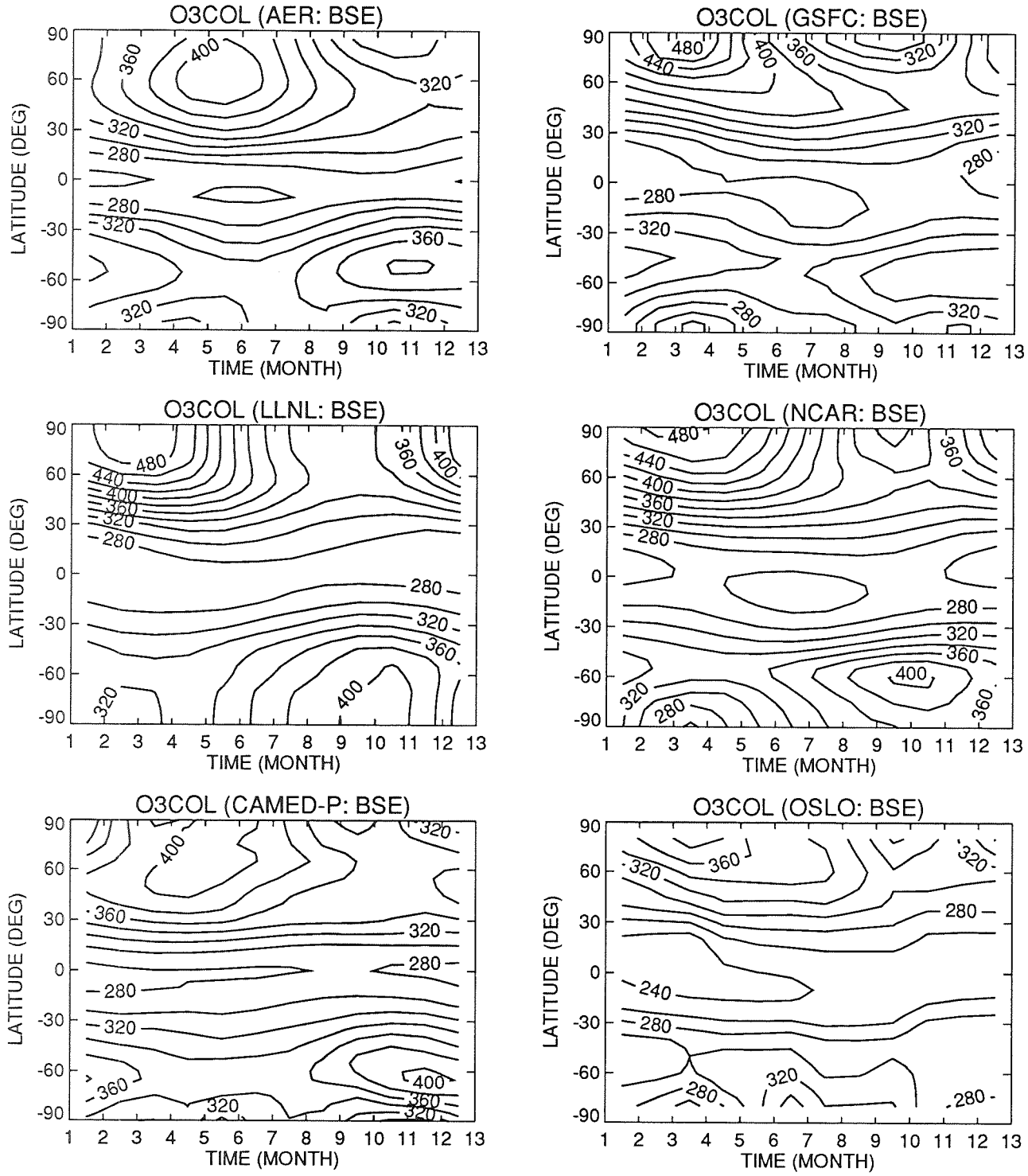

Figure 4. Calculated column abundances of O_3 (Dobson units) for the baseline case (BSE) from the different models.

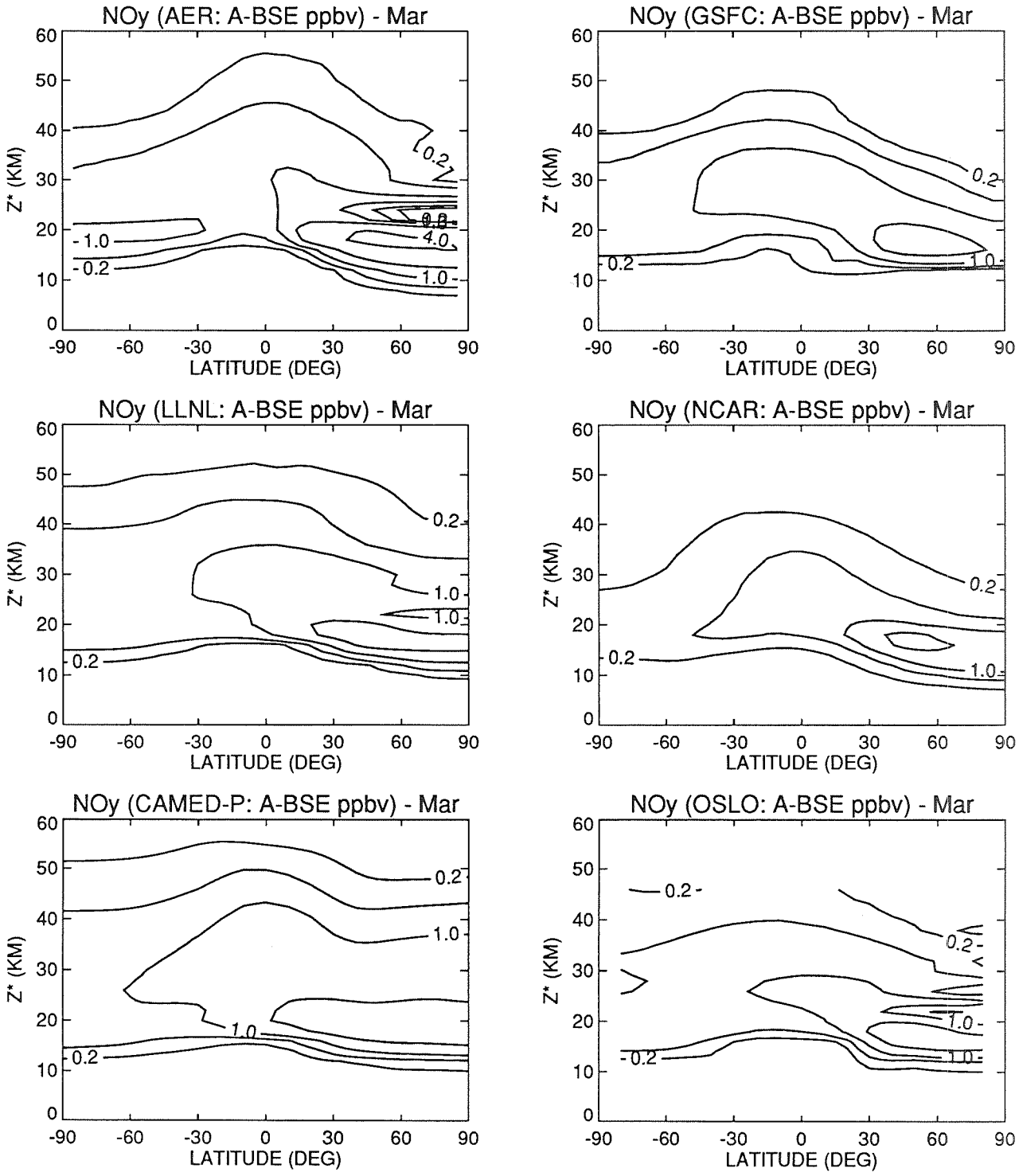

Figure 5(a). Calculated changes in the concentrations of NO_y in parts per billion by volume for March in case A relative to the baseline (BSE). The contours are 0.2, 0.5, 1.0, 2.0, and 4.0 ppbv.

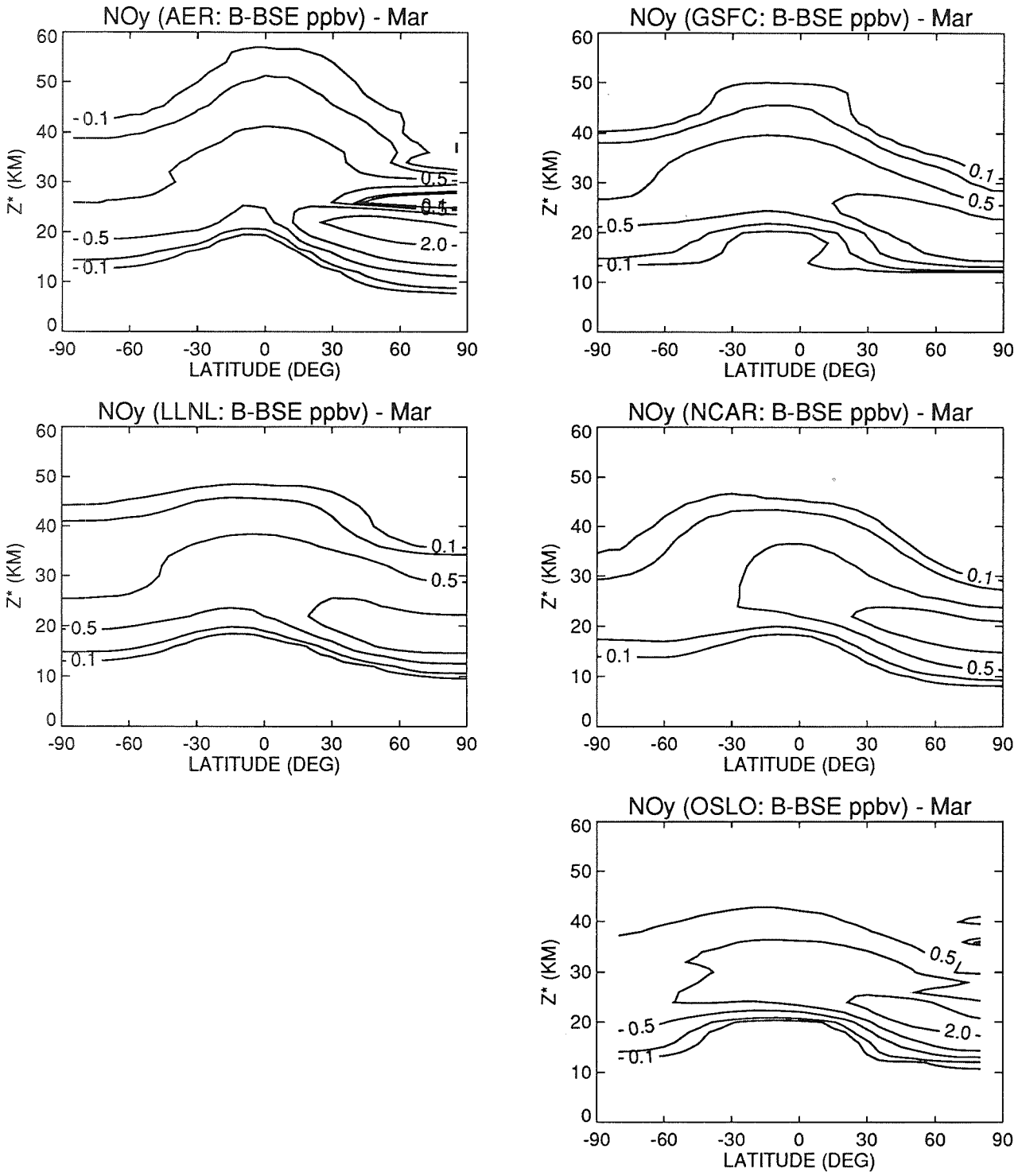

Figure 5(b). Calculated changes in the concentrations of NO_y in parts per billion by volume for March in case B relative to the baseline (BSE). The contours are 0.1, 0.2, 0.5,1.0, 2.0, and 4.0 ppbv.

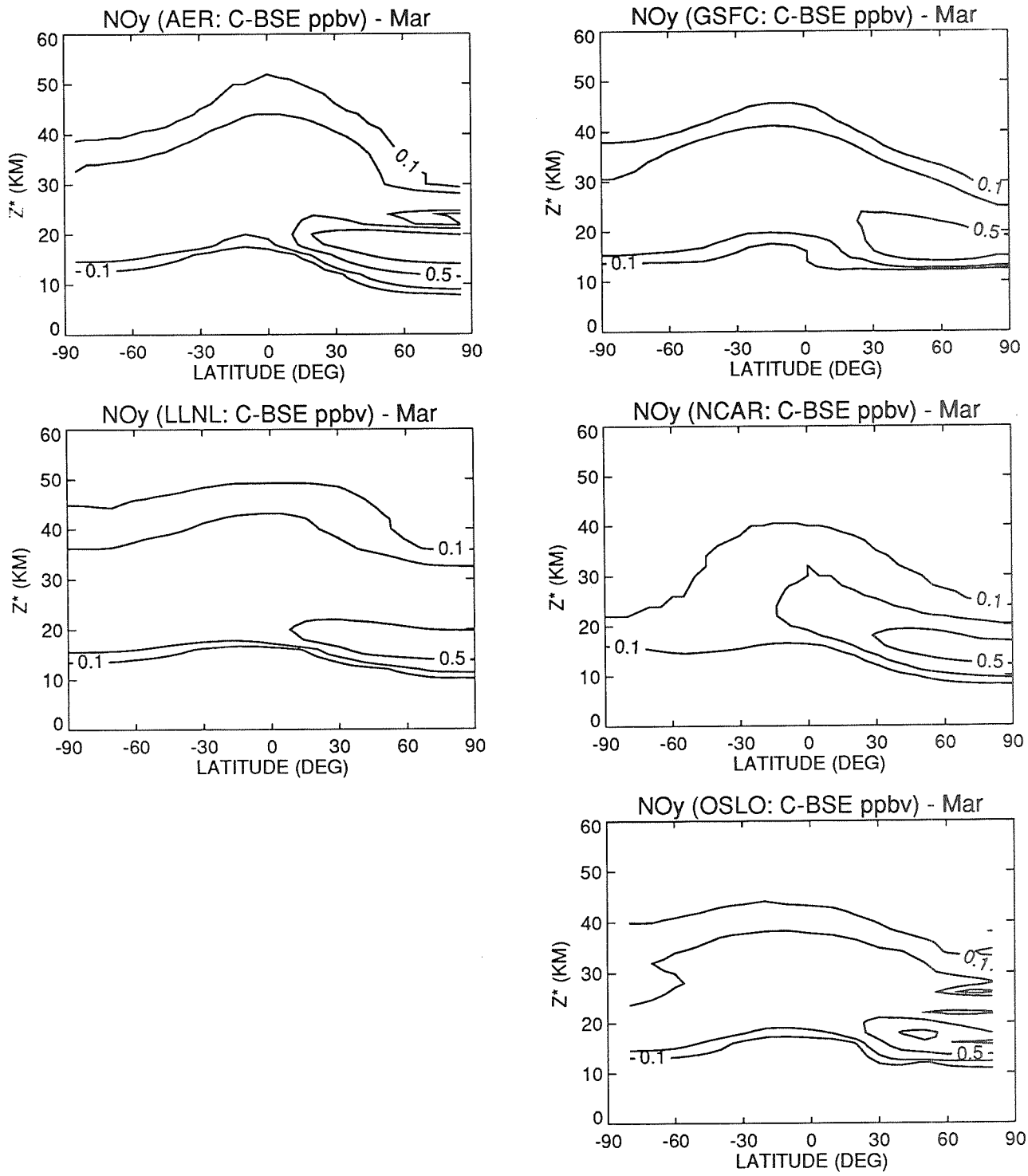

Figure 5(c). Calculated changes in the concentrations of NO_y in parts per billion by volume for March in case C, relative to the baseline (BSE). The contours are 0.1, 0.2, 0.5,1.0, 2.0, and 4.0 ppbv.

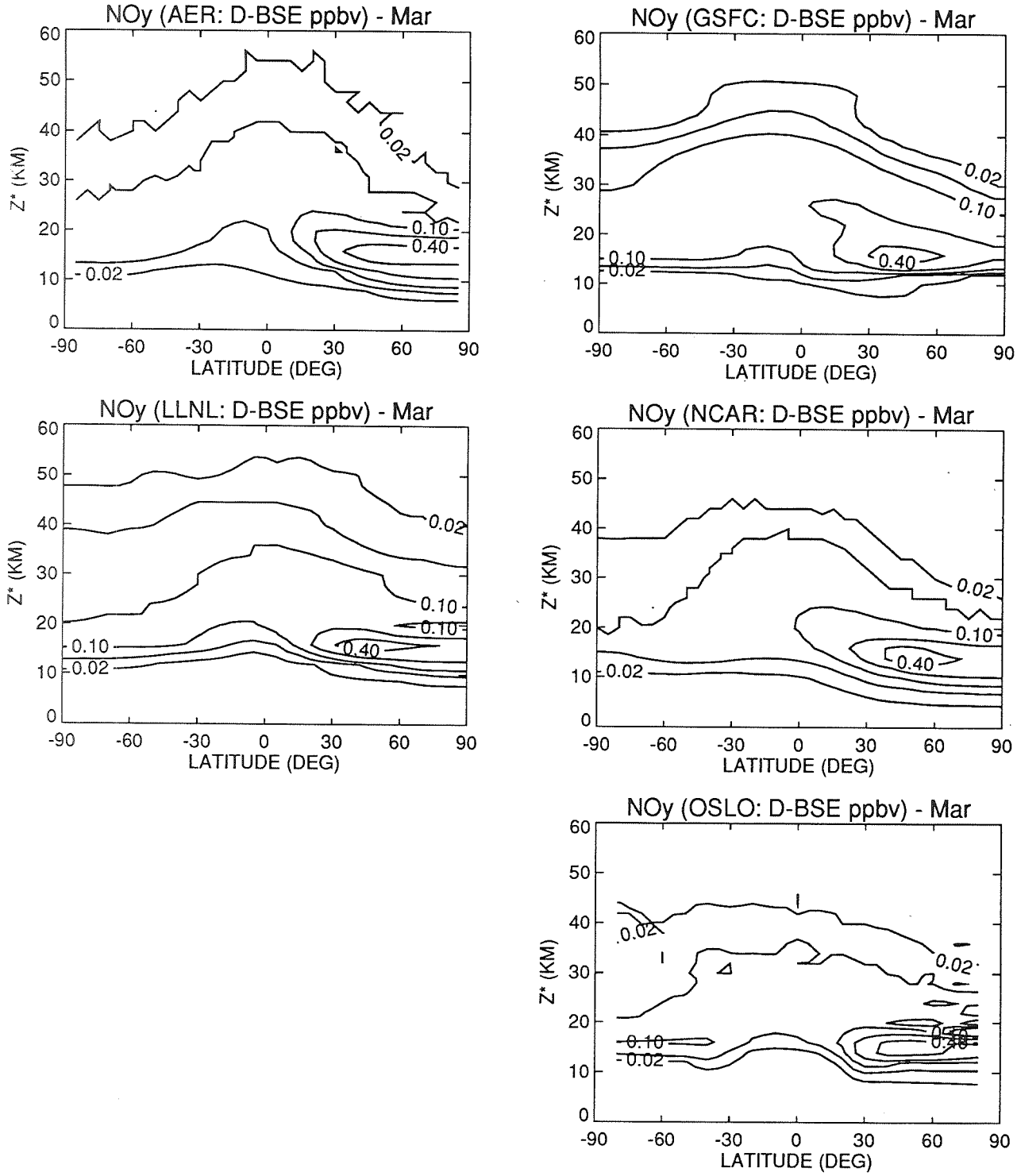

Figure 5(d). Calculated changes in the concentrations of NO_y in parts per billion by volume for March in case D, relative to the baseline (BSE). The contours are 0.02, 0.05, 0.1, 0.2, and 0.4 ppbv.

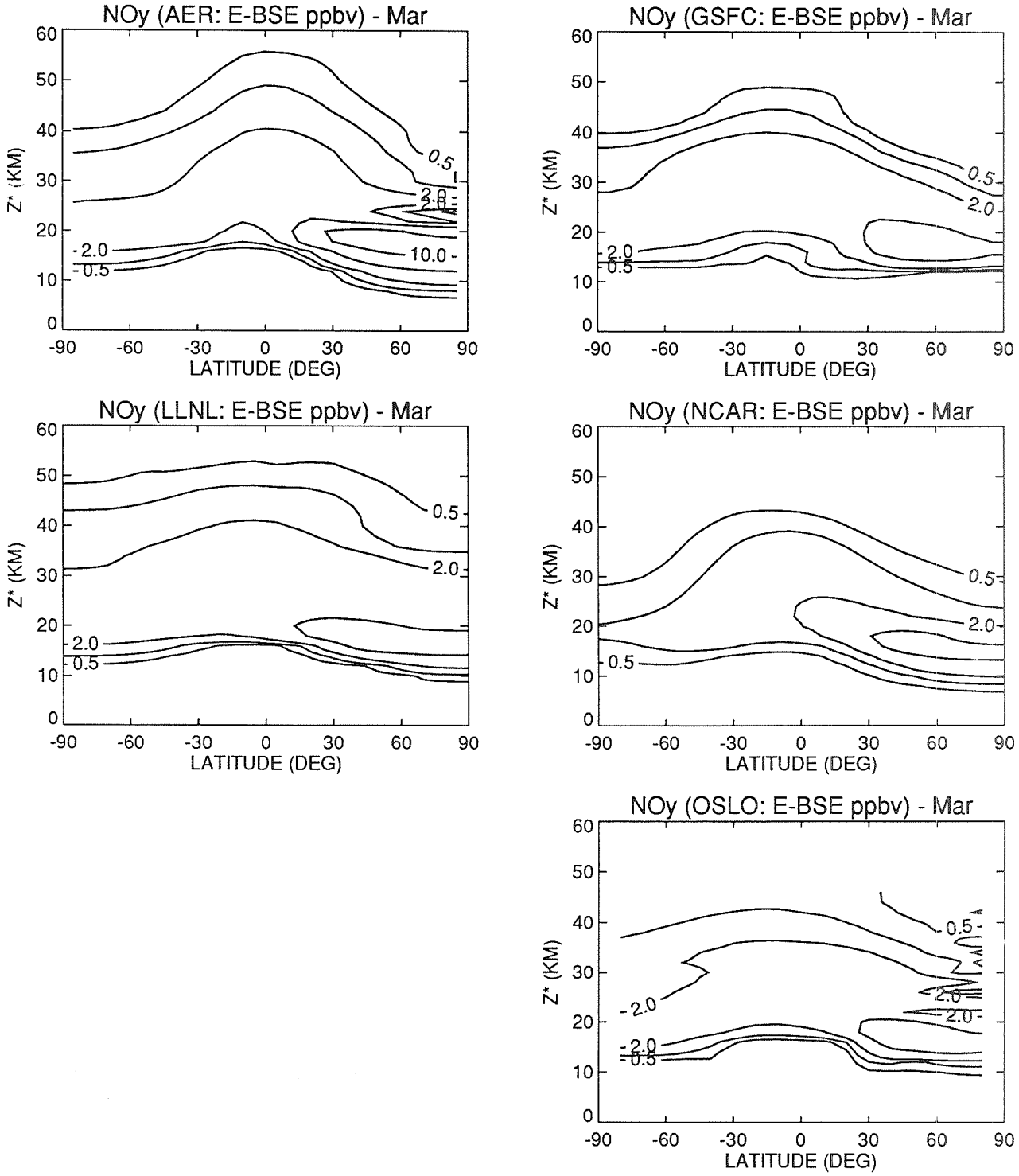

Figure 5(e). Calculated changes in the concentrations of NO_y in parts per billion by volume for March in case E, relative to the baseline (BSE). The contours are 0.5,1.0, 2.0 , 5.0, and 10.0 ppbv.

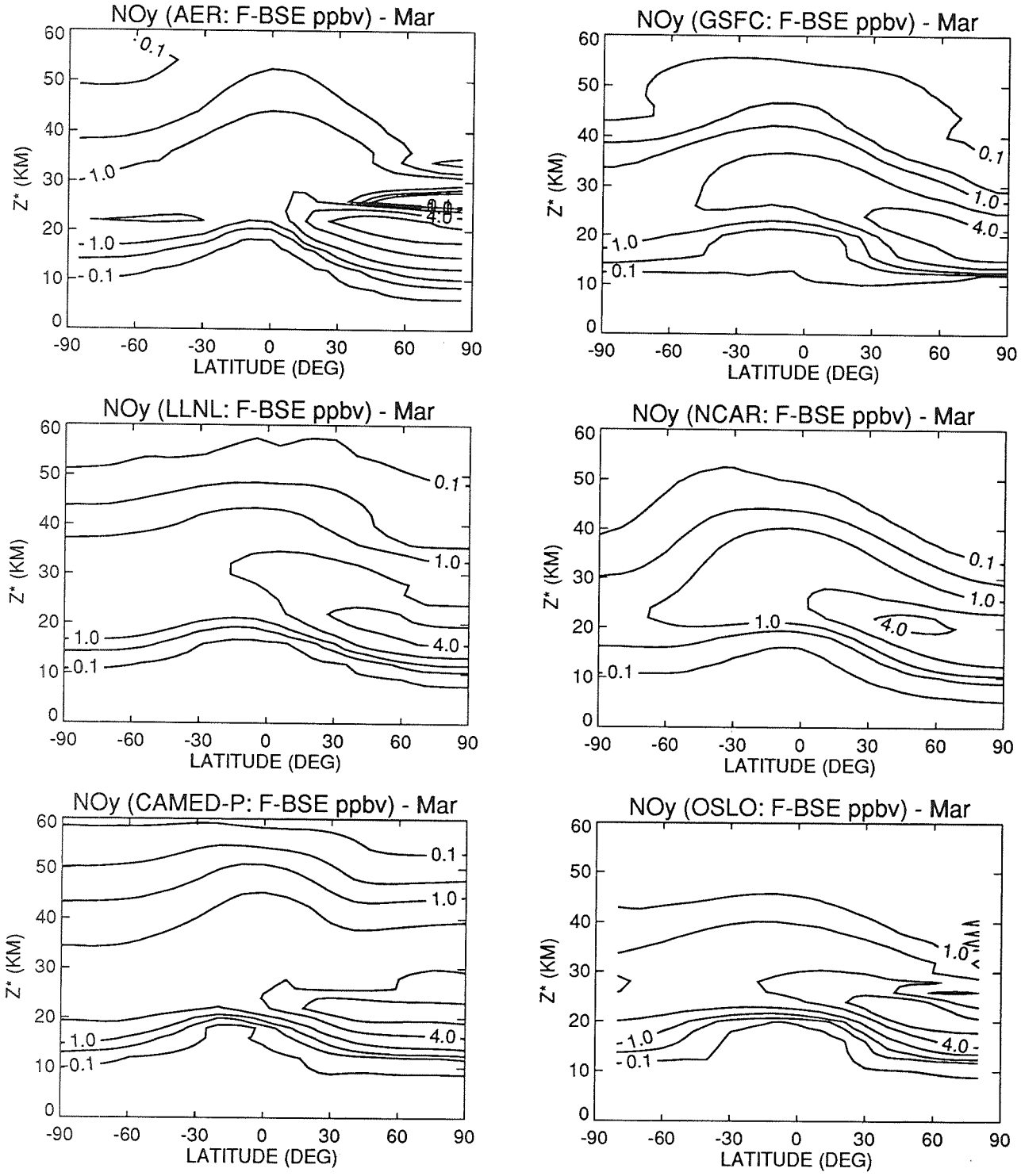

Figure 5(f). Calculated changes in the concentrations of NO_y in parts per billion by volume for March in case F, relative to the baseline (BSE). The contours are 0.1, 0.5, 1.0, 2.0, 4.0, and 6.0 ppbv.

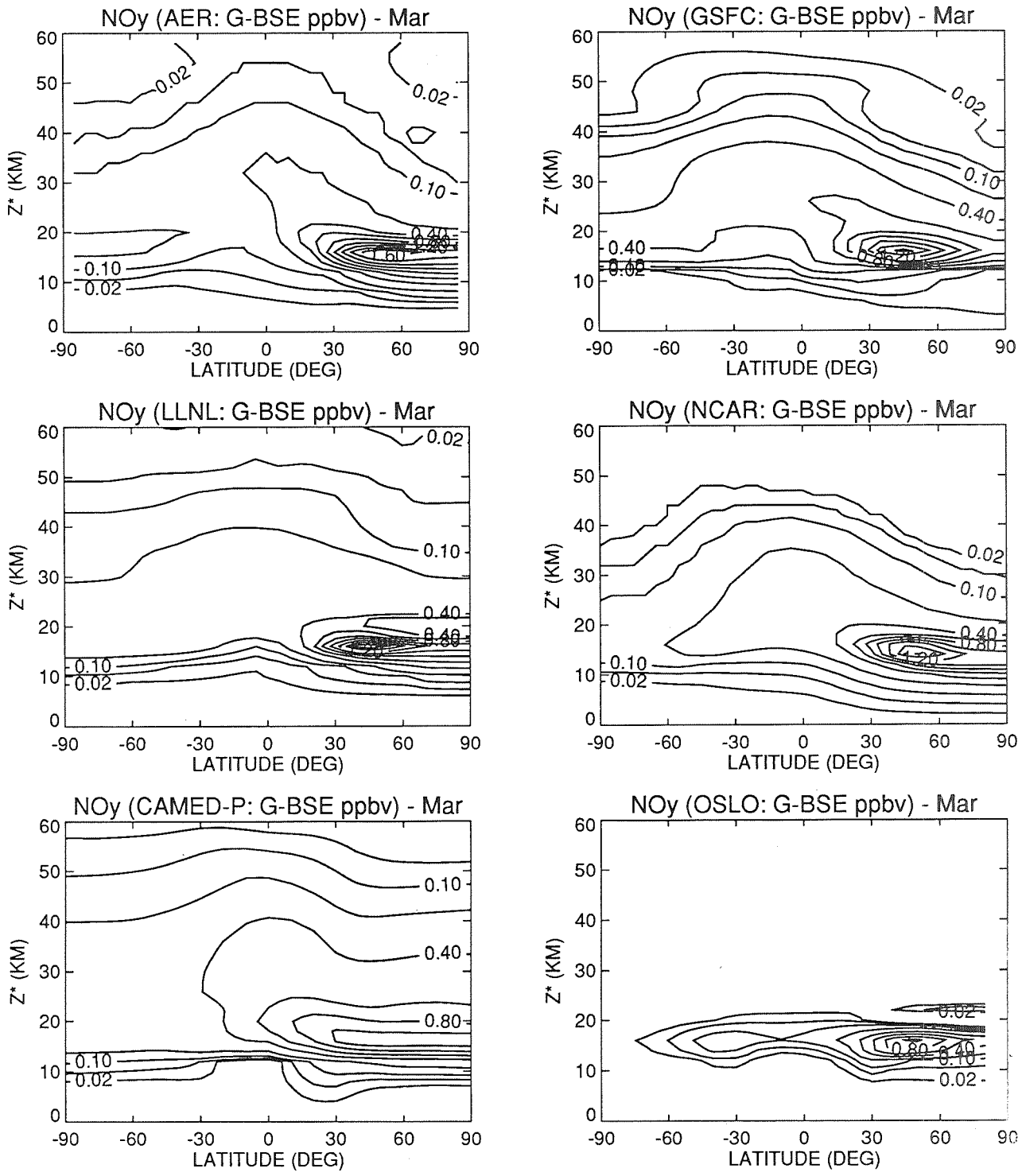

Figure 5(g). Calculated changes in the concentrations of NO_y in parts per billion by volume for March in case G, relative to the baseline (BSE). The contours are 0.02, 0.05, 0.1, and 0.2, in steps of 0.2 ppbv.

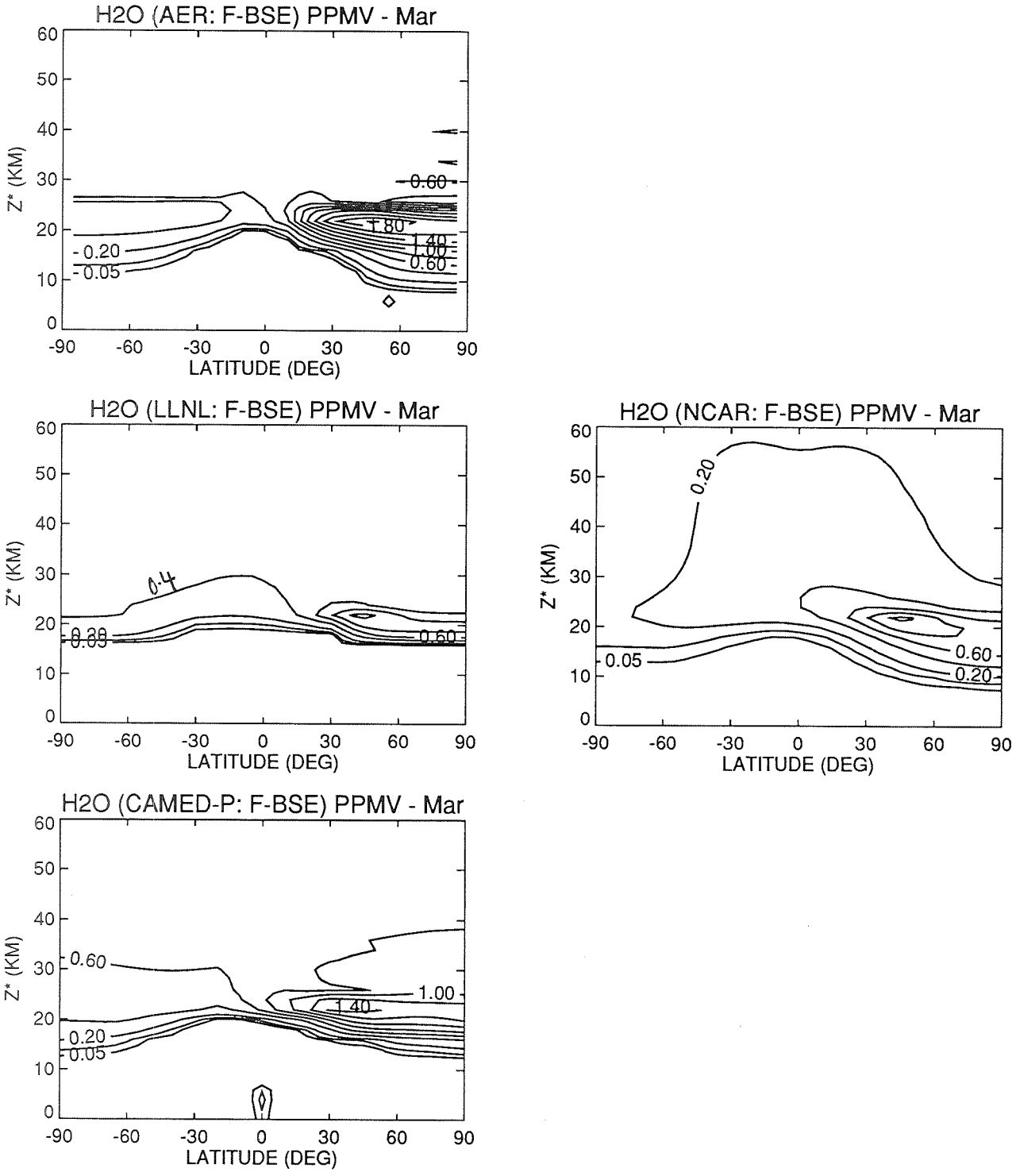

Figure 6. Calculated changes in the concentrations of H_2O in parts per million by volume for March in case F, relative to the baseline (BSE). The contours are 0.05, 0.1, 0.2, and 0.4, in steps of 0.2 ppmv.

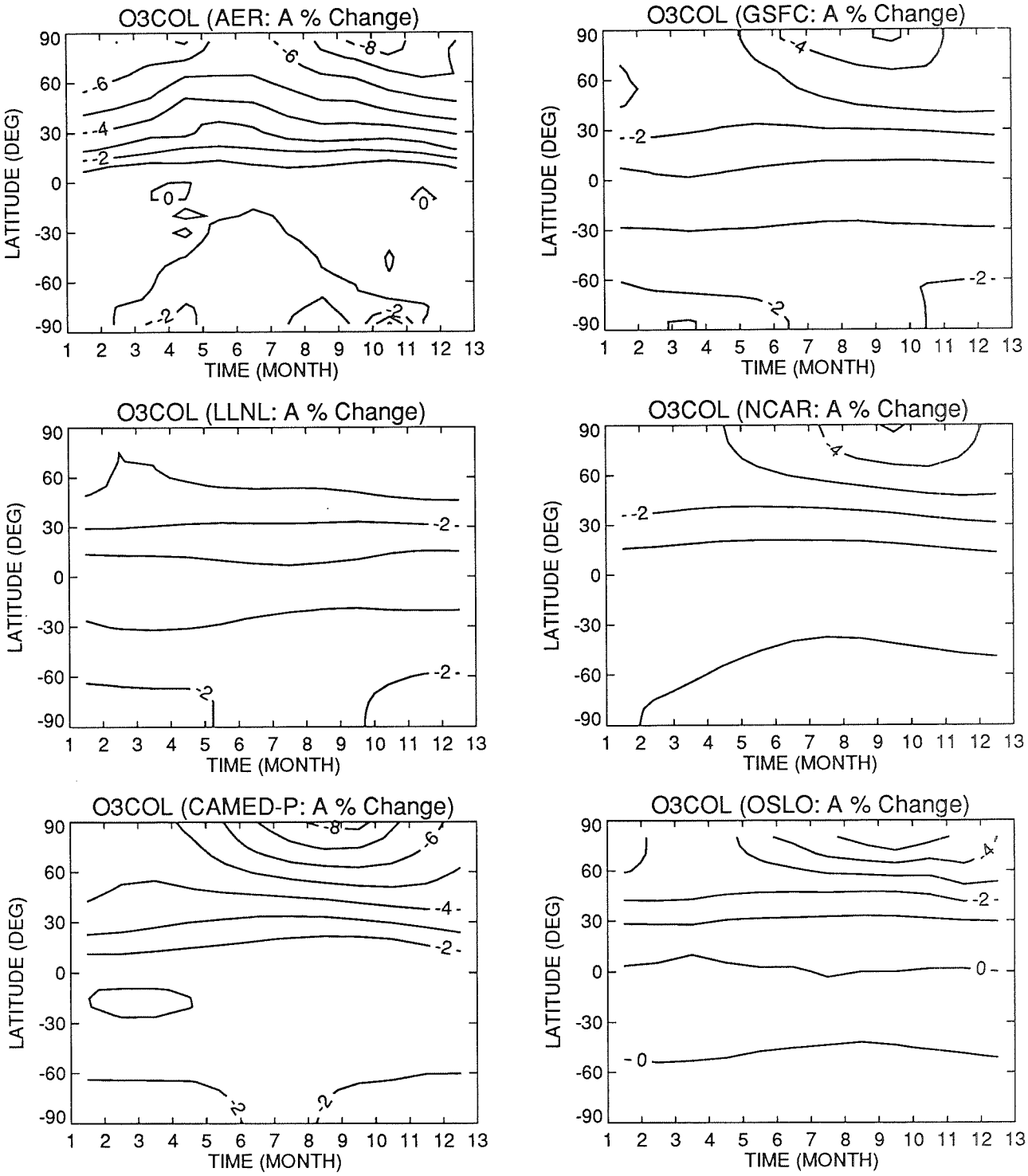

Figure 7(a). Calculated percent changes in the column abundances of O_3 as functions of latitude and season in case A, relative to the baseline (BSE). The contours are 2%, 1%, 0%, -1.0%, to -8.0%, in steps of -1%.

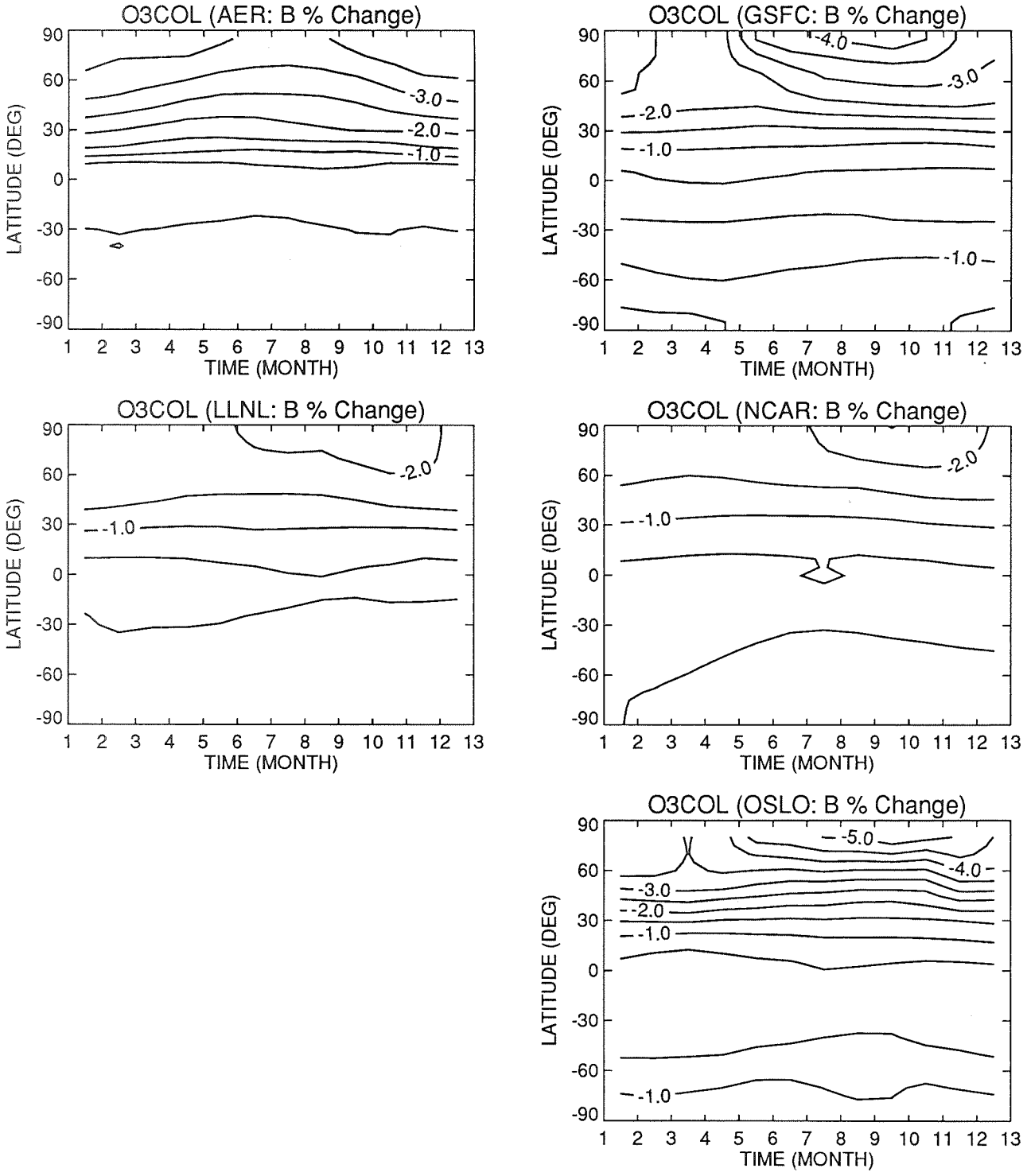

Figure 7(b). Calculated percent changes in the column abundances of O_3 as functions of latitude and season in case B, relative to the baseline (BSE). The contours are -0.5, -1.0,-1.5, -2.0, etc., in steps of 0.5%.

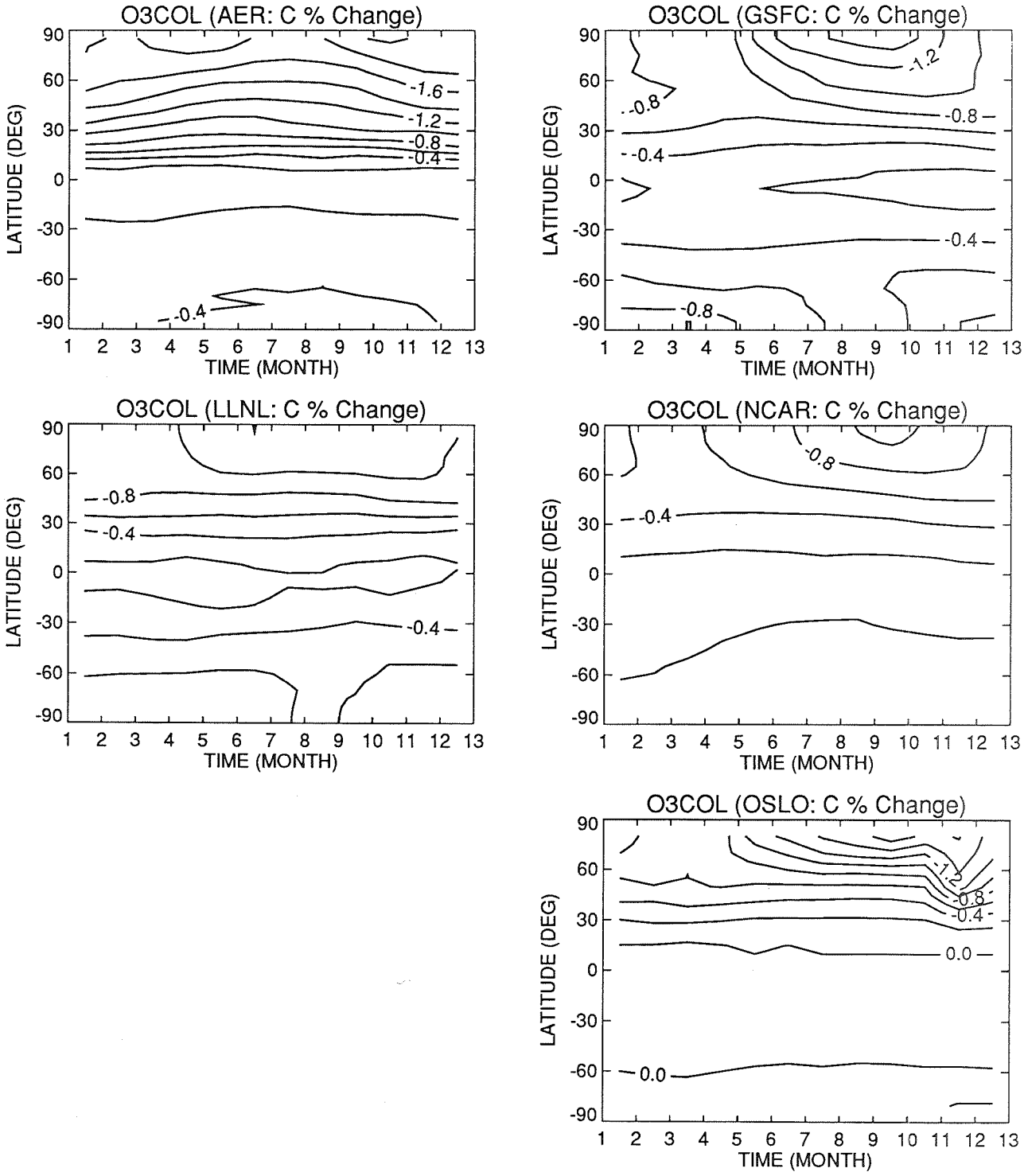

Figure 7(c). Calculated percent changes in the column abundances of O_3 as functions of latitude and season in case C, relative to the baseline (BSE). The contours are 0.0, -0.2, -0.4, etc., in steps of 0.2%.

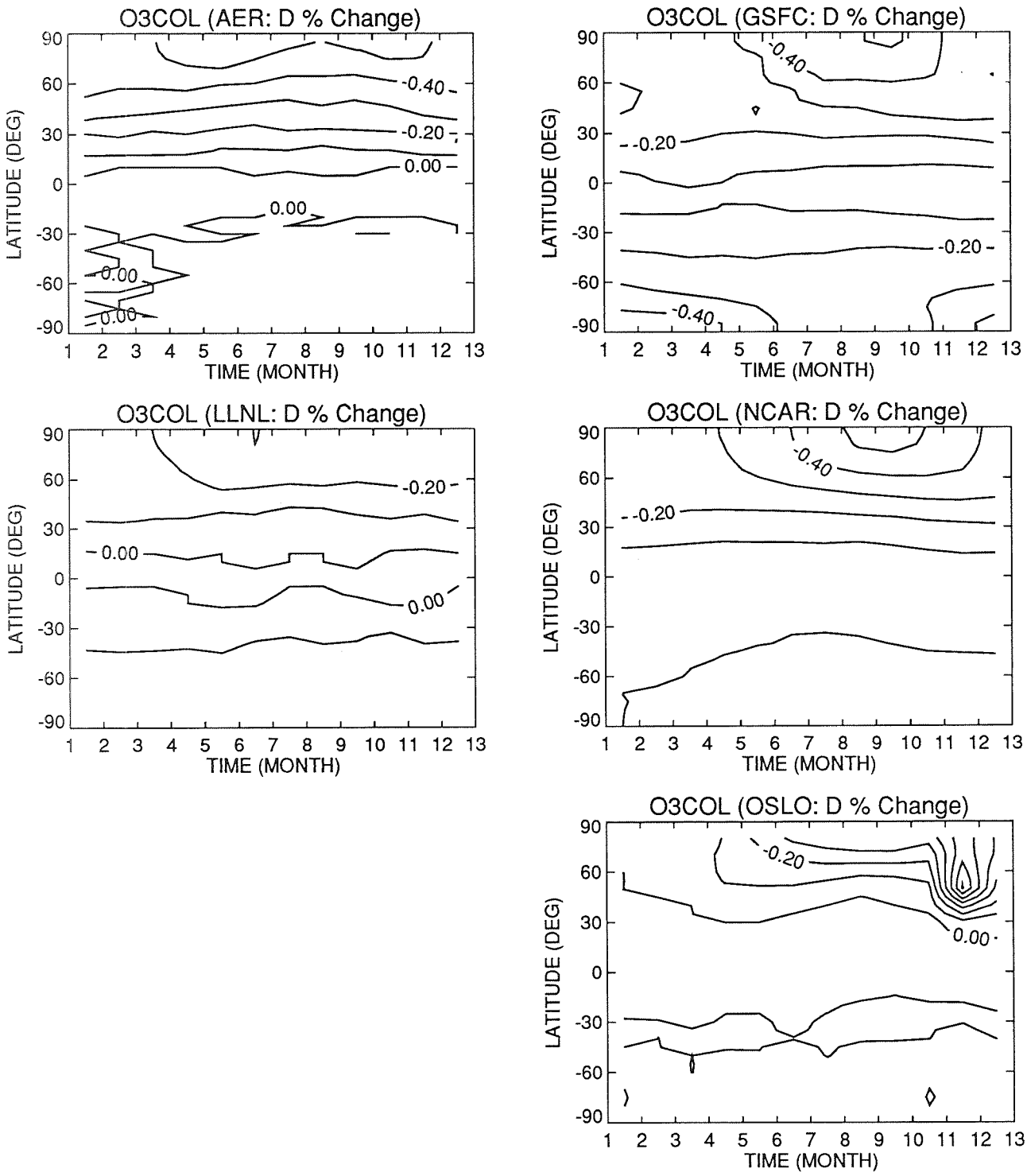

Figure 7(d). Calculated percent changes in the column abundances of O_3 as functions of latitude and season in case D, relative to the baseline (BSE). The contours are 0., -0.1, -0.2, etc., in steps of 0.1%.

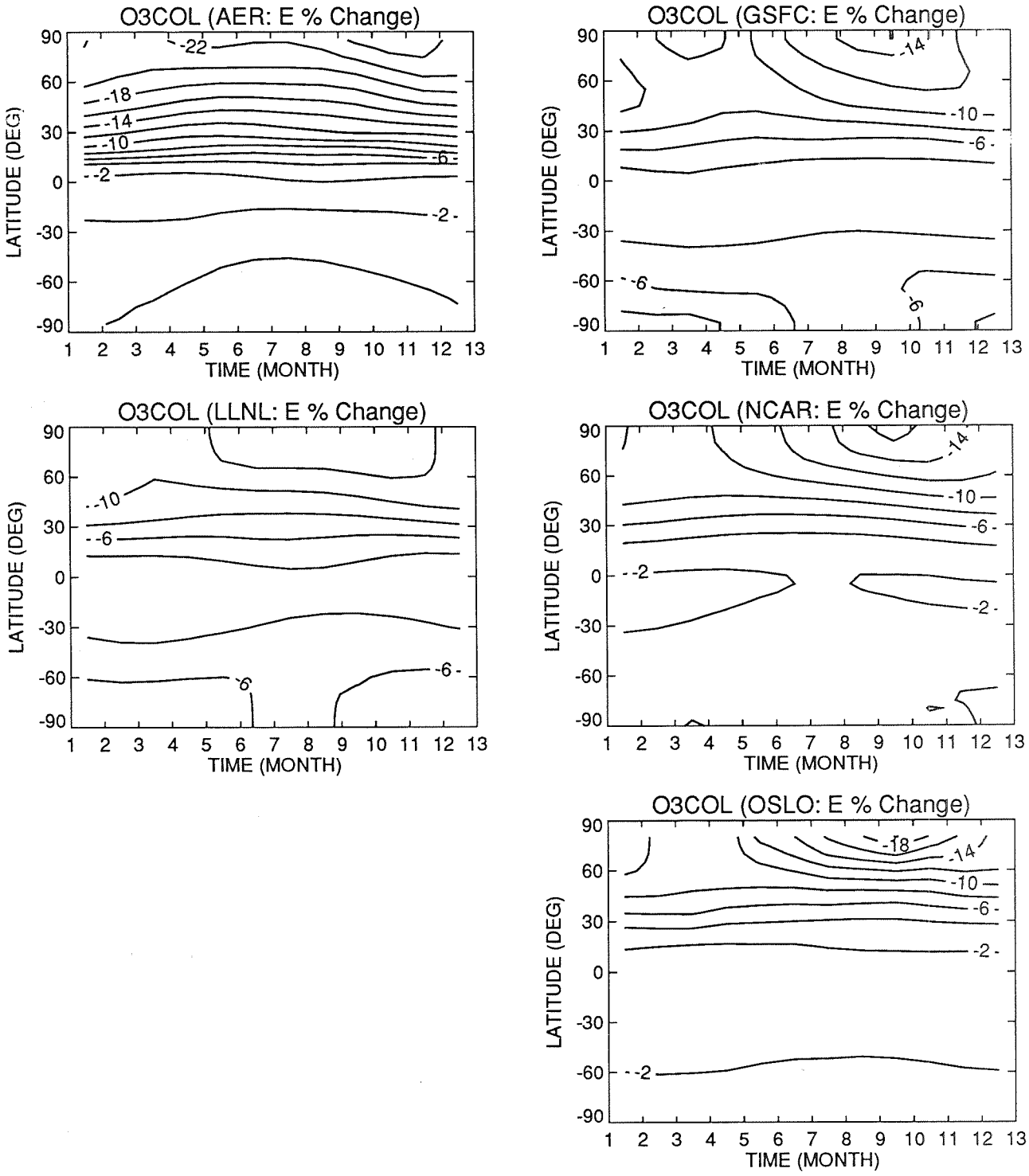

Figure 7(e). Calculated percent changes in the column abundances of O_3 as functions of latitude and season in case E, relative to the baseline (BSE). The contours are -2.0, -4.0, -6.0, etc., in steps of 2.0%.

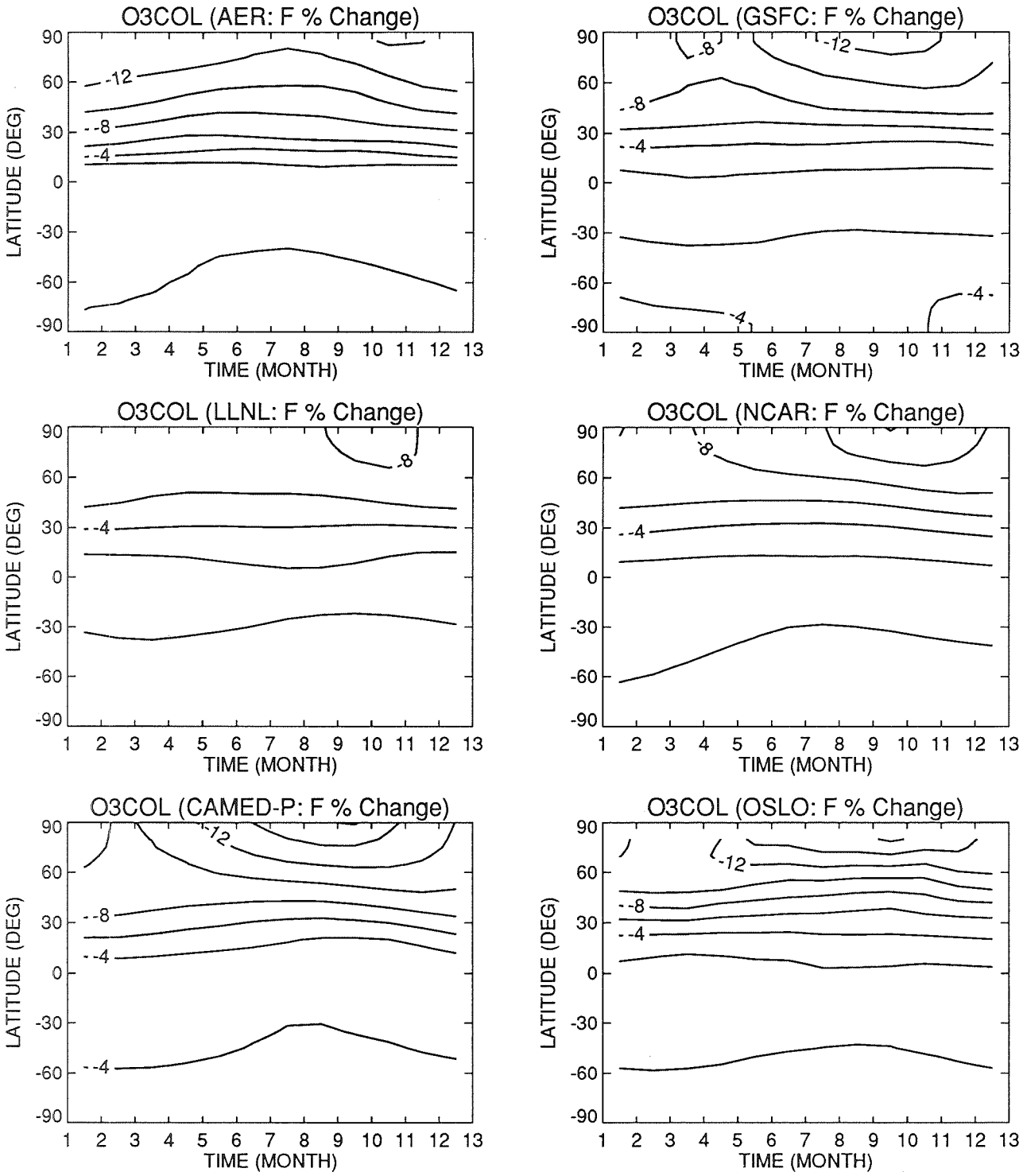

Figure 7(f). Calculated percent changes in the column abundances of O_3 as functions of latitude and season in case F, relative to the baseline (BSE). The contours are +2, 0, -2.0, -4.0, -6.0, etc., in steps of 2.0%.

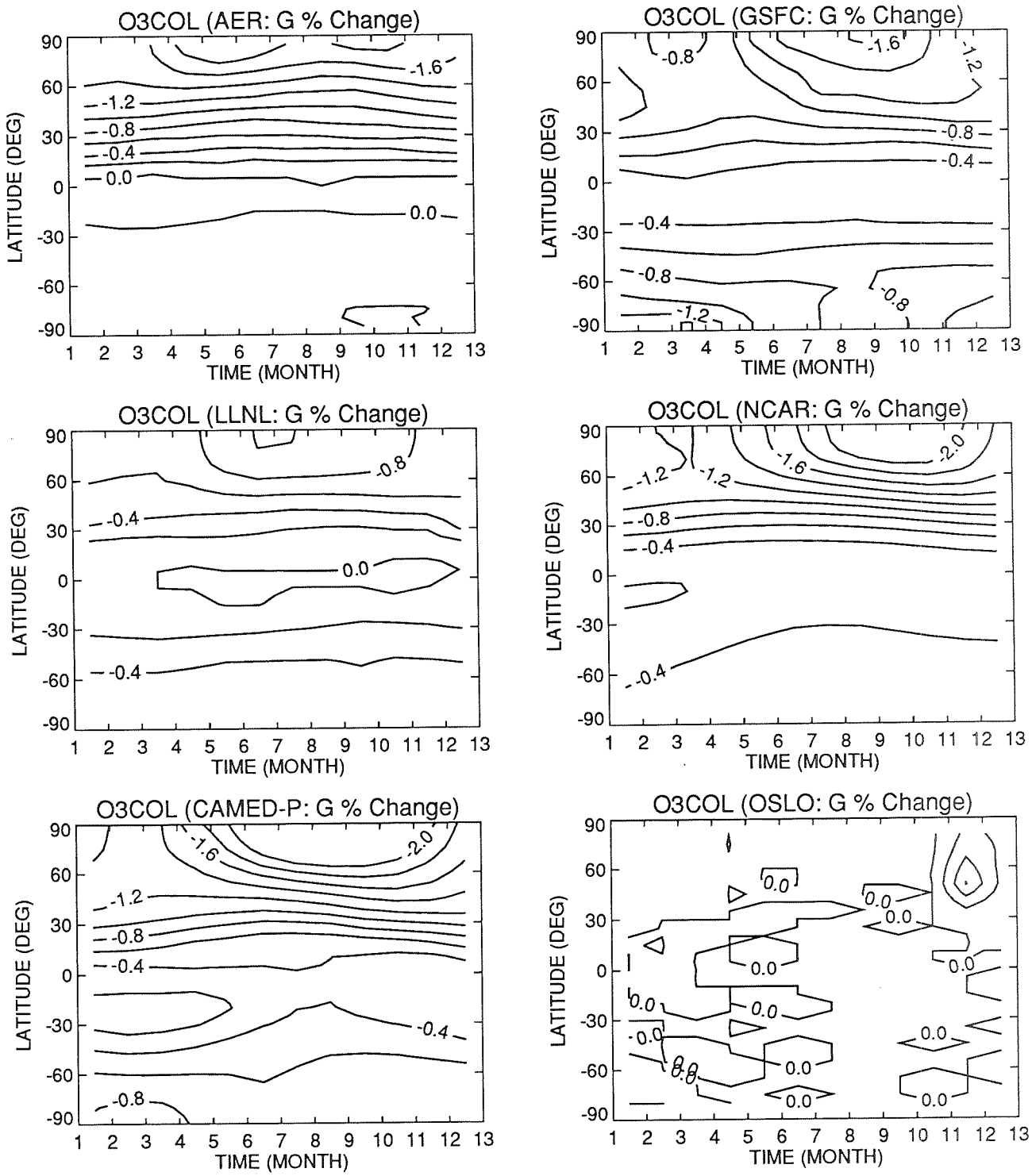

Figure 7(g). Calculated percent changes in the column abundances of O_3 as functions of latitude and season in case G, relative to the baseline (BSE). The contours are 0., -0.2, -0.4, -0.6, etc., in steps of 0.2%.

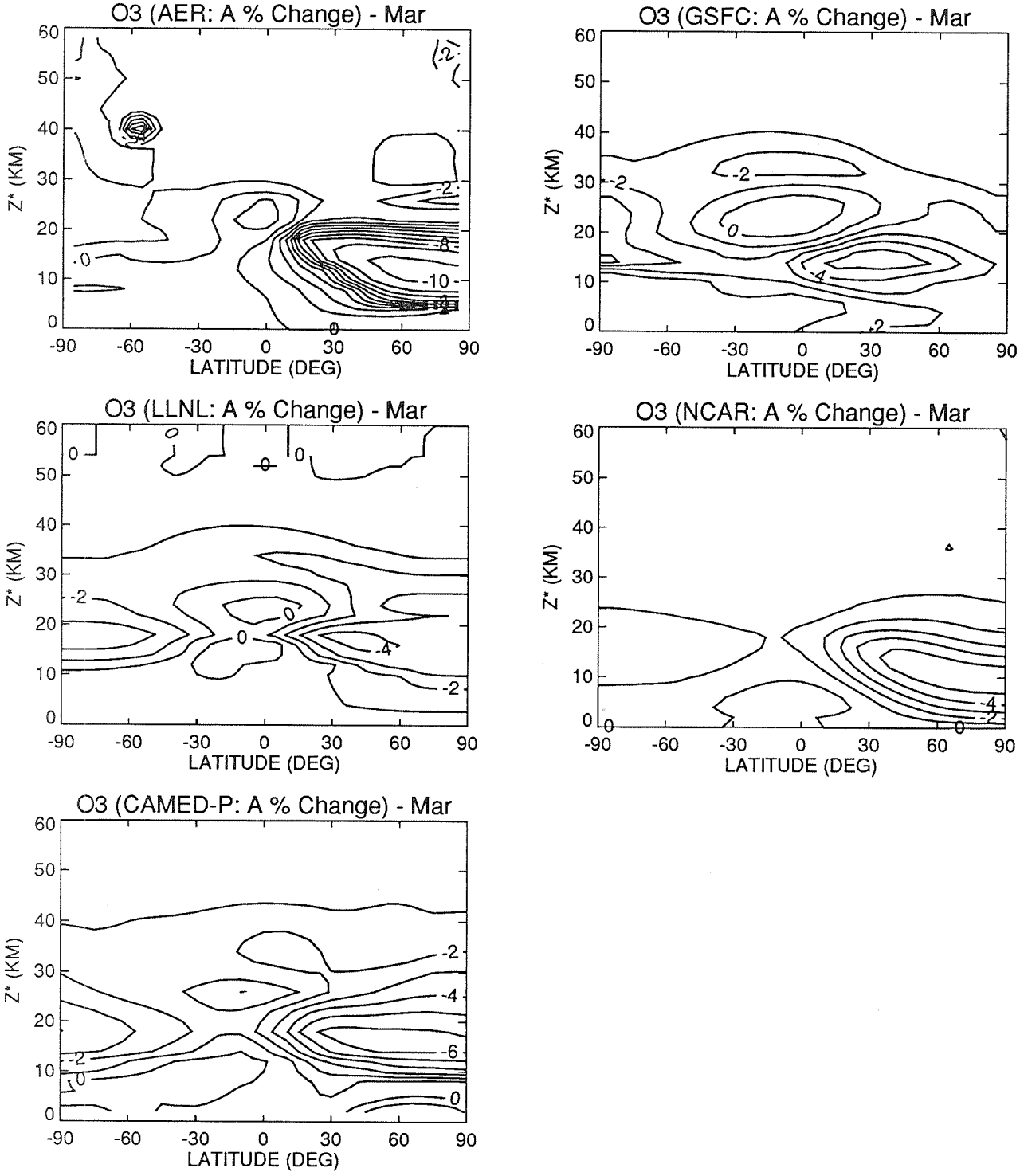

Figure 8(a). Calculated percent changes in the local concentration of O_3 as functions of latitude and height in case A, relative to the baseline (BSE). The contours are +1, 0., -1.0, -2.0, -3.0, etc., in steps of 1.0%.

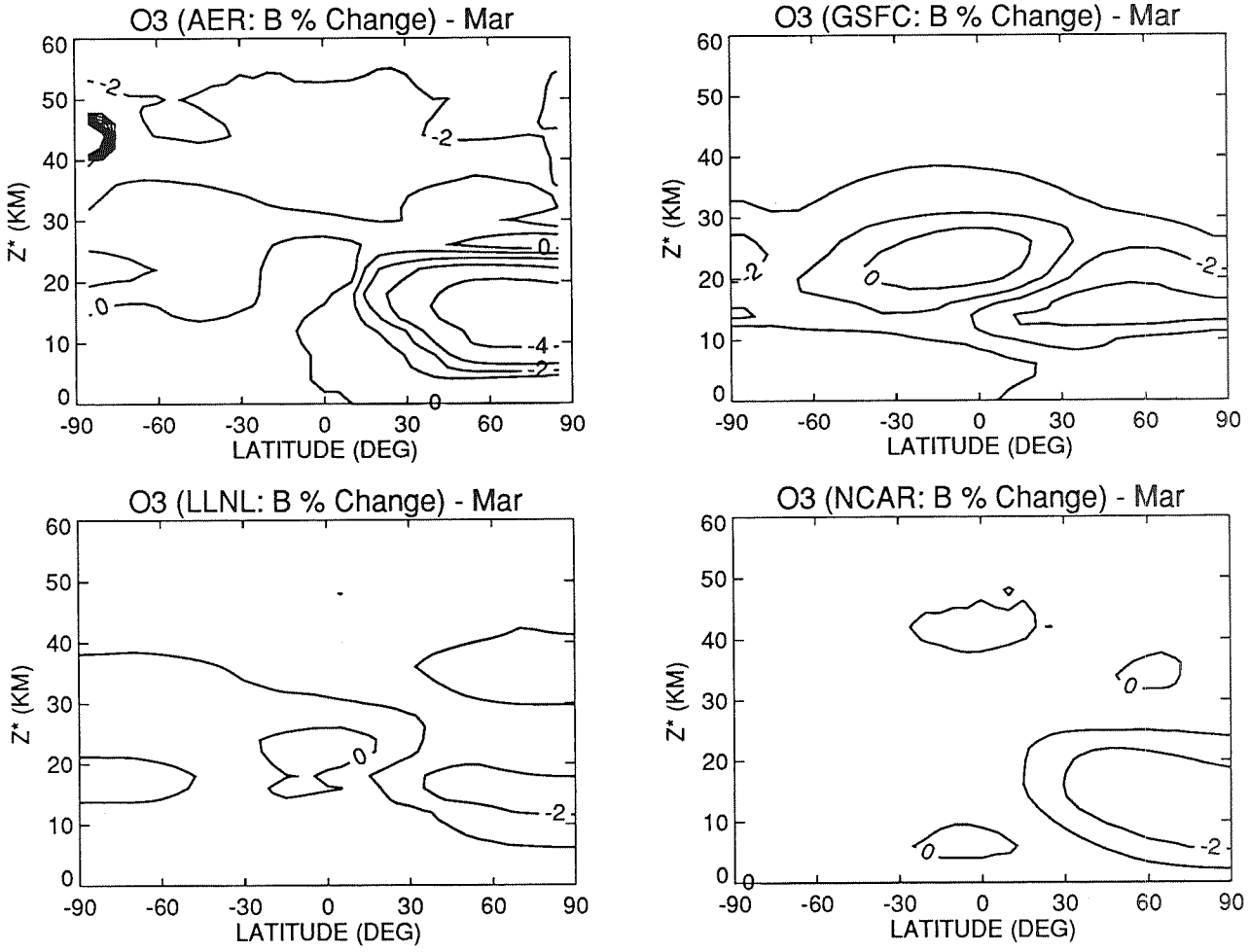

Figure 8(b). Calculated percent changes in the local concentration of O_3 as functions of latitude and height in case B, relative to the baseline (BSE). The contours are +1, 0., -1.0, -2.0, -3.0, etc., in steps of 1.0%.

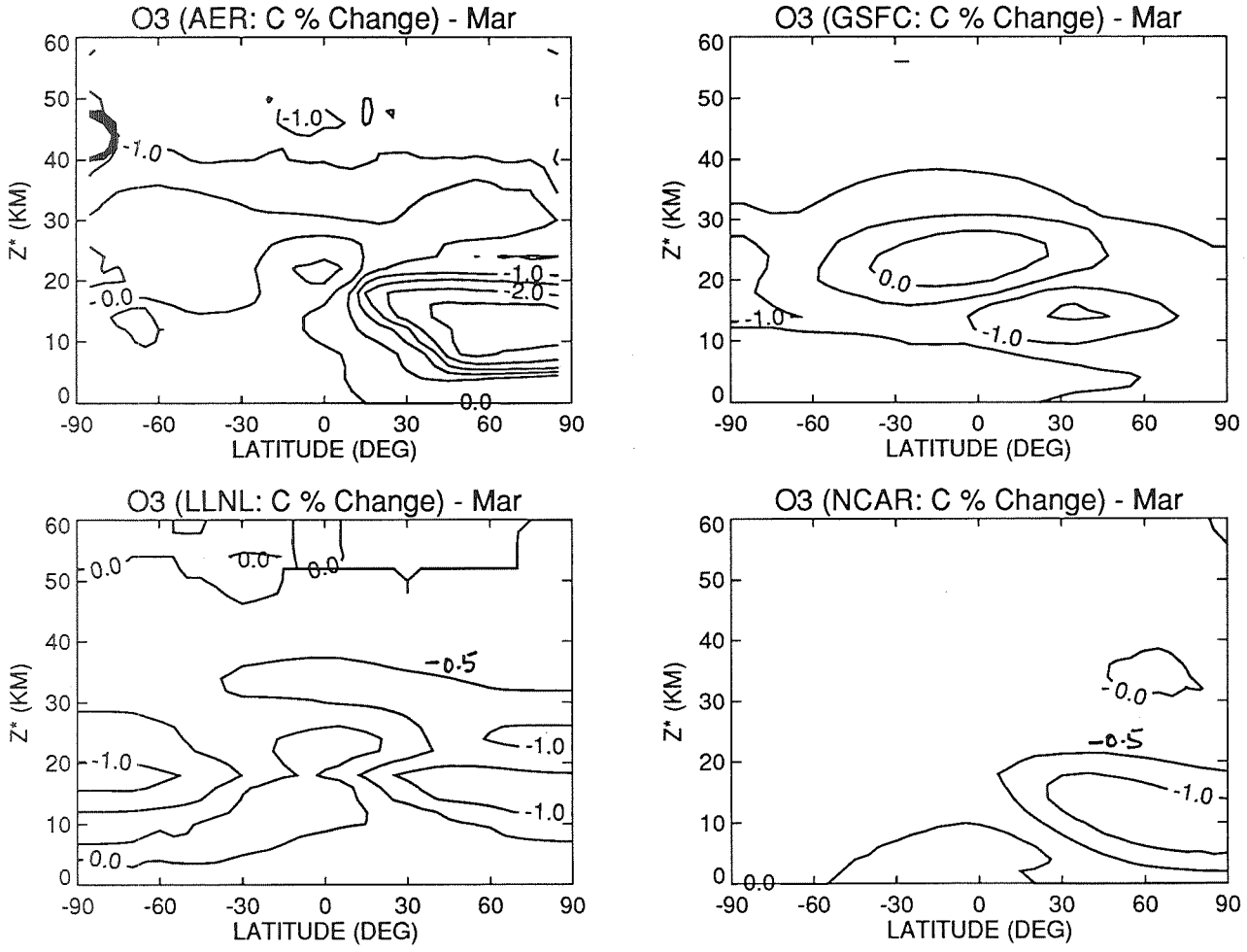

Figure 8(c). Calculated percent changes in the local concentration of O_3 as functions of latitude and height in case C, relative to the baseline (BSE). The contours are 0.5, 0., -0.5, -1.0, -1.5, etc., in steps of 0.5%.

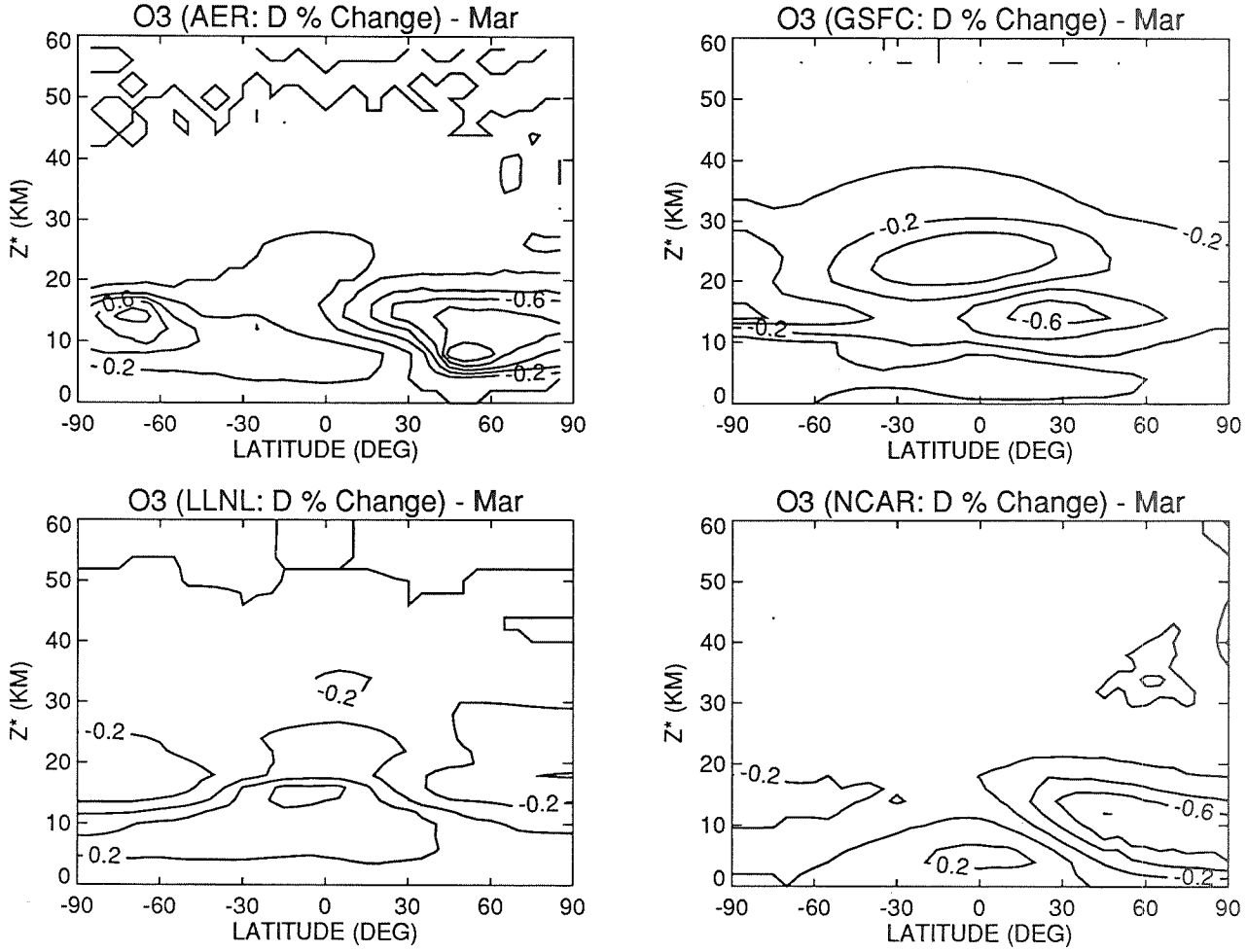

Figure 8(d). Calculated percent changes in the local concentration of O_3 as functions of latitude and height in case D, relative to the baseline (BSE). The contours are +0.8 to -1.0, in steps of 0.2%.

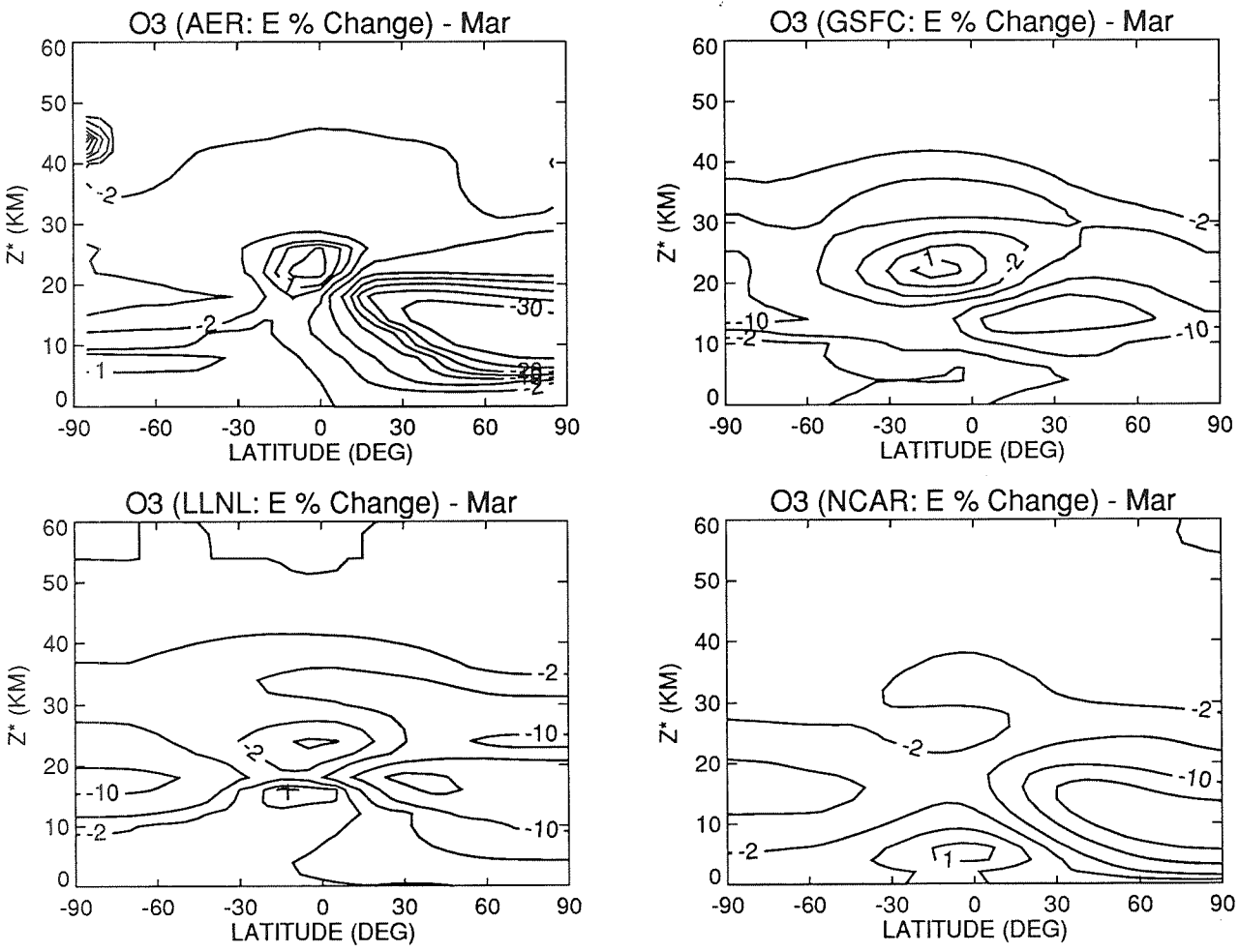

Figure 8(e). Calculated percent changes in the local concentration of O_3 as functions of latitude and height in case E, relative to the baseline (BSE). The contours are +2, +1, 0., -2.0, -5.0, -10, -15, etc., in steps of 5.0%.

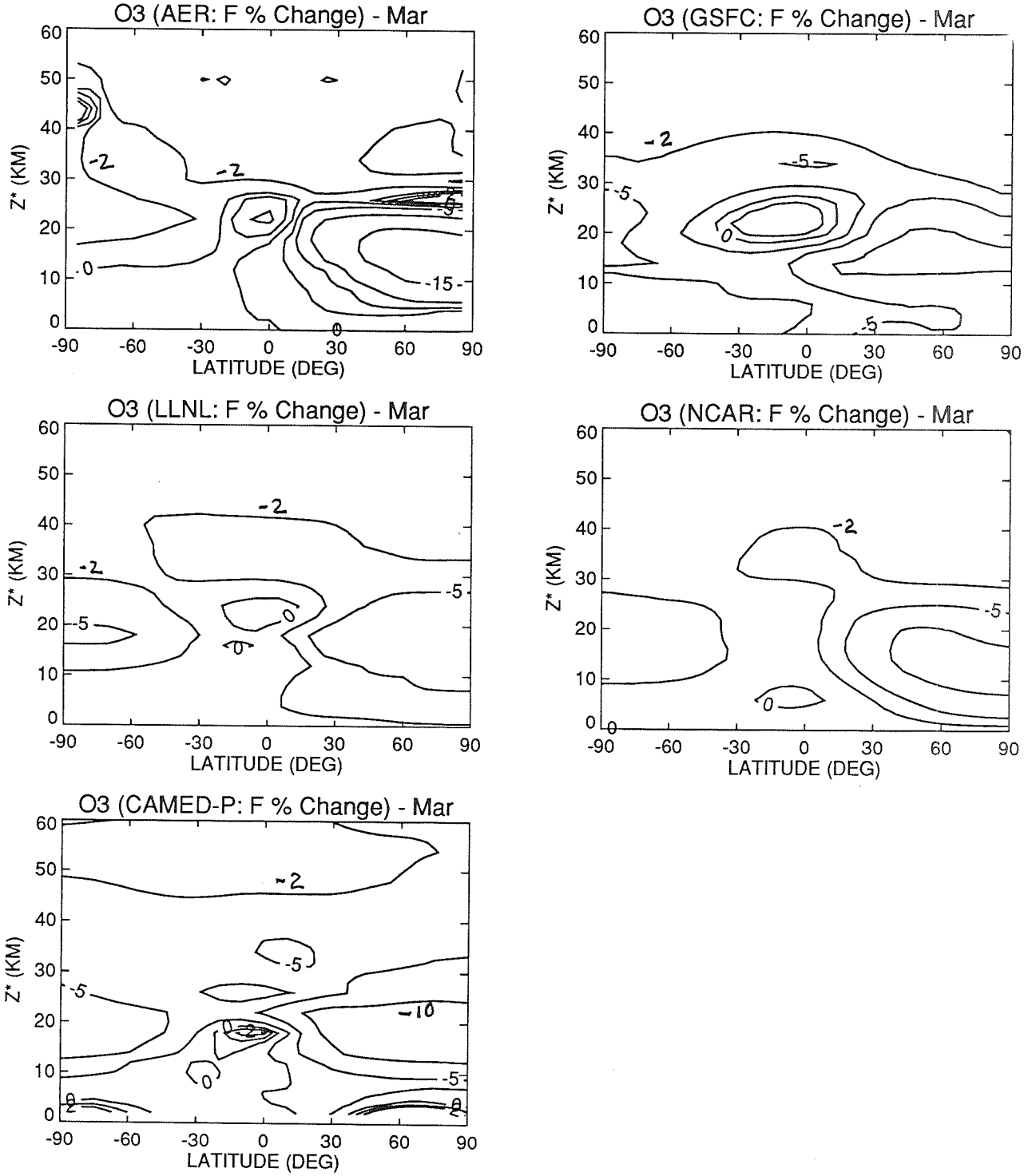

Figure 8(f). Calculated percent changes in the local concentration of O_3 as functions of latitude and height in case F, relative to the baseline (BSE). The contours are +2, +1, 0., -2.0, -5.0, -10, and -15.0%.

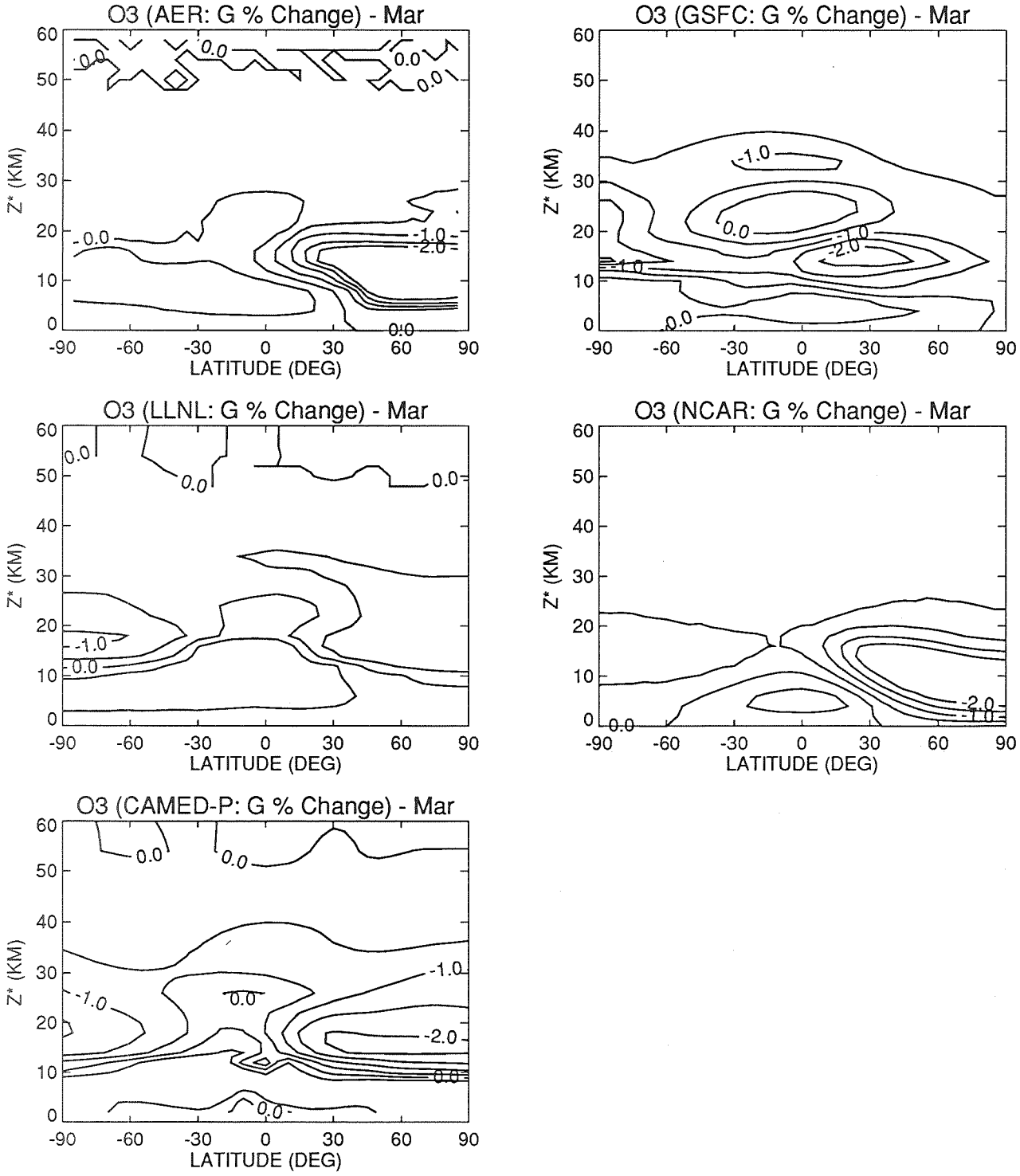

Figure 8(g). Calculated percent changes in the local concentration of O_3 as functions of latitude and height in case G, relative to the baseline (BSE). The contours are +0.5, 0, -1.0, -1.5, and -2.0%.

REFERENCES

1. Boeing Commercial Airplanes, "High-Speed Civil Transport Study, Summary," NASA Contractor Report 4234. Boeing Commercial Airplanes, New Airplane Development, 1989."

2. Douglas Aircraft Company, "Study of High-Speed Civil Transport," NASA Contractor Report 4235. Douglas Aircraft Company, New Commercial Programs, 1989.

3. Johnston, H.S., D.E. Kinnison, and D.J. Wuebbles, Nitrogen oxides from high-altitude aircraft: An update of potential effects on ozone. *J. Geophys. Res., 94,* 16351-16363, 1989.

4. Ko, M.K., D.K. Weisenstein, N.-D. Sze, R.-L. Shia, J.M. Rodriguez, and C. Heisey, "Effects of Engine Emissions from High Speed-Civil Transport Aircraft: A Two-Dimensional Modeling Study, Part I." Final Report for ST Systems Corporation for period July 1, 1988 through June 30, 1989, 1991.

5. Ko, M.K., D.K. Weisenstein, N.-D. Sze, R.-L. Shia, J.M. Rodriguez, and C. Heisey, "Effects of Engine Emissions from High Speed Civil Transport Aircraft: A Two-Dimensional Modeling Study, Part II." Final Report for ST Systems Corporation for period July 1, 1989 through Dec. 31, 1989, 1991.

6. Johnston, H.S., M.J. Prather, and R.T. Watson, *The Atmospheric Effects of Stratospheric Aircraft: A Topical Review,* NASA Reference Publication 1250, National Aeronautics and Space Administration, Office of Management, Scientific and Technical Information Division, 1991.

7. Douglass, A.R., M.A. Carroll, W.B. DeMore, J.R. Holton, I.S.A. Isaksen, H.S. Johnston, and M.K.W. Ko, *The Atmospheric Effects of Stratospheric Aircraft: A Current Consensus,* NASA Reference Publication 1251 National Aeronautics and Space Administration, Office of Management, Scientific and Technical Information Division, 1991.

8. Jackman, C.H., R.K. Seals, and M.J. Prather, Editors, *Two-Dimensional Intercomparison of Stratospheric Models,* NASA Conference Publication 3042, Proceedings of a workshop sponsored by NASA, Washington, D.C., Upper Atmosphere Theory and Data Analysis Program held in Virginia Beach, VA Sept. 11-16, 1988, 1989.

9. WMO, Scientific Assessment of Stratospheric Ozone: 1989. World Meteorological Organization, Global Ozone Research and Monitoring Project -Report No. 20, 1990.